Cell Metabolism
Clinical and Translational Report

Dual impacts of serine/glycine-free diet in enhancing antitumor immunity and promoting evasion via PD-L1 lactylation

Graphical abstract

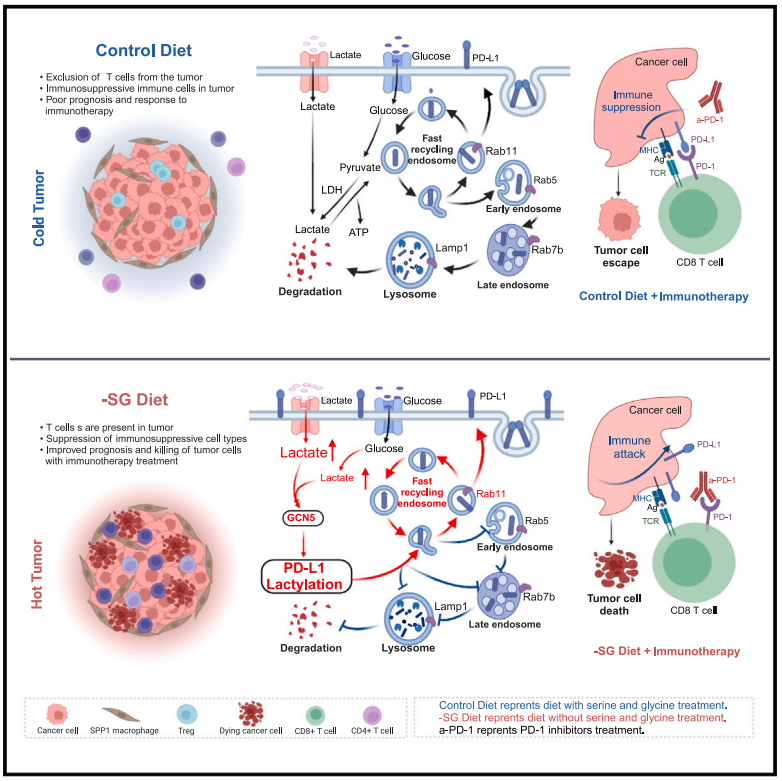

Highlights

- Serine/glycine-free diet inhibits tumor growth and enhances antitumor immunity
- PD-L1 lactylation delays the degradation of PD-L1 in tumor cells by lysosome
- PD-L1 lactylation provides a potential target for immunotherapy
- Serine/glycine-free diet is proven feasible and safe in clinical trial

Authors

Huan Tong, Zedong Jiang, Linlin Song, ..., Zhen Lei, Hubing Shi, Xuelei Ma

Correspondence

zlei@rplushealth.com (Z.L.), shihb@scu.edu.cn (H.S.), drmaxuelei@gmail.com (X.M.)

In brief

The serine/glycine-free diet inhibits CRC growth and enhances antitumor immunity but also promotes immune evasion through PD-L1 lactylation. It shows promise when combined with immunotherapy and has been proven feasible and safe in a single-arm, phase I trial.

Tong et al., 2024, Cell Metabolism *36*, 2493–2510
December 3, 2024
https://doi.org/10.1016/j.cmet.2024.10.019

CellPress

Cell Metabolism

CellPress
OPEN ACCESS

Clinical and Translational Report

Dual impacts of serine/glycine-free diet in enhancing antitumor immunity and promoting evasion via PD-L1 lactylation

Huan Tong,[1,13] Zedong Jiang,[1,2,13] Linlin Song,[3,4,13] Keqin Tan,[5,13] Xiaomeng Yin,[1,13] Chengyuan He,[6,13] Juan Huang,[7,13] Xiaoyue Li,[1,8] Xiaofan Jing,[9] Hong Yun,[1] Guangqi Li,[1] Yunuo Zhao,[1] Qianlong Kang,[1,2] Yuhao Wei,[1] Renwei Li,[1] Zhiwen Long,[6] Jun Yin,[6] Qiang Luo,[10] Xiao Liang,[1] Yanzhi Wan,[3] Aiping Zheng,[11] Nan Lin,[1] Tao Zhang,[1] Jiayi Xu,[12] Xinggang Yang,[1] Yuting Jiang,[1] Yueyi Li,[1] Yu Xiang,[1] Yu Zhang,[1] Lusi Feng,[1] Zhen Lei,[6,*] Hubing Shi,[3,*] and Xuelei Ma[1,14,*]

[1]Department of Biotherapy, Cancer Center and State Key Laboratory of Biotherapy, West China Hospital, Sichuan University, Chengdu, Sichuan, China
[2]Frontiers Science Center for Disease-related Molecular Network, West China Hospital, Sichuan University, Chengdu, Sichuan, China
[3]Laboratory of Integrative Medicine, Clinical Research Center for Breast, State Key Laboratory of Biotherapy, West China Hospital, Sichuan University and Collaborative Innovation Center, Chengdu, Sichuan, China
[4]Department of Ultrasound & Laboratory of Ultrasound Medicine, West China Hospital, Sichuan University, Chengdu, Sichuan, China
[5]Division of Abdominal Tumor Multimodality Treatment, Cancer Center, West China Hospital, Sichuan University, Chengdu, Sichuan, China
[6]Recovery Plus Clinic, New York, NY 10019, USA
[7]Department of Hematology, Sichuan Academy of Medical Sciences and Sichuan Provincial People's Hospital, University of Electronic Science and Technology of China, Chengdu, Sichuan, China
[8]Wupai Technology Limited Liability Company, Chengdu, Sichuan, China
[9]Department of Nutrition, West China Hospital, Sichuan University, Chengdu, Sichuan, China
[10]Department of Oncology, Xinjin District Hospital of Traditional Chinese Medicine, Chengdu, Sichuan, China
[11]Division of Head & Neck Tumor Multimodality Treatment, Cancer Center, West China Hospital, Sichuan University, Chengdu, Sichuan, China
[12]Core Facilities, West China Hospital, Sichuan University, Chengdu, Sichuan, China
[13]These authors contributed equally
[14]Lead contact
*Correspondence: zlei@rplushealth.com (Z.L.), shihb@scu.edu.cn (H.S.), drmaxuelei@gmail.com (X.M.)
https://doi.org/10.1016/j.cmet.2024.10.019

SUMMARY

The effect of the serine/glycine-free diet (−SG diet) on colorectal cancer (CRC) remains unclear; meanwhile, programmed death-1 (PD-1) inhibitors are less effective for most CRC patients. Here, we demonstrate that the −SG diet inhibits CRC growth and promotes the accumulation of cytotoxic T cells to enhance antitumor immunity. Additionally, we also identified the lactylation of programmed death-ligand 1 (PD-L1) in tumor cells as a mechanism of immune evasion during cytotoxic T cell-mediated antitumor responses, and blocking the PD-1/PD-L1 signaling pathway is able to rejuvenate the function of CD8+ T cells recruited by the −SG diet, indicating the potential of combining the −SG diet with immunotherapy. We conducted a single-arm, phase I study (ChiCTR2300067929). The primary outcome suggests that the −SG diet is feasible and safe for regulating systemic immunity. Secondary outcomes include patient tolerability and potential antitumor effects. Collectively, our findings highlight the promising therapeutic potential of the −SG diet for treating solid tumors.

INTRODUCTION

Colorectal cancer (CRC) is the third prevalent cancer globally with increasing mortality rate.[1,2] The Food and Drug Administration (FDA) has approved immune checkpoint inhibitors (ICIs) therapy for CRC treatment, including programmed death-1 (PD-1) inhibitors, yet over 85% patients with mismatch repair proficient/microsatellite stable (pMMR/MSS) characteristics can hardly benefit from this.[3–7] In contrast, deficient mismatch repair/microsatellite stability high (d-MMR/MSI-H) CRC, which demonstrates a complete response to PD-1 inhibitors, exhibits a higher tumor neoantigen load[8,9] and greater infiltration of immune cells compared with pMMR/MSS.[10–14] The lack of immune cell infiltration in pMMR/MSS CRC underscores its resistance to immunotherapy, suggesting that modulating the immune state could be the key point to enhance the efficacy of immunotherapy for these patients.

Cancer cells demonstrate a heightened metabolic status, relying on exogenous serine, glycine, and other amino acids to support their initiation, proliferation, metastasis, and resistance.[15–23] This process is primarily driven by anaerobic glycolysis, producing large amounts of lactate, which fosters

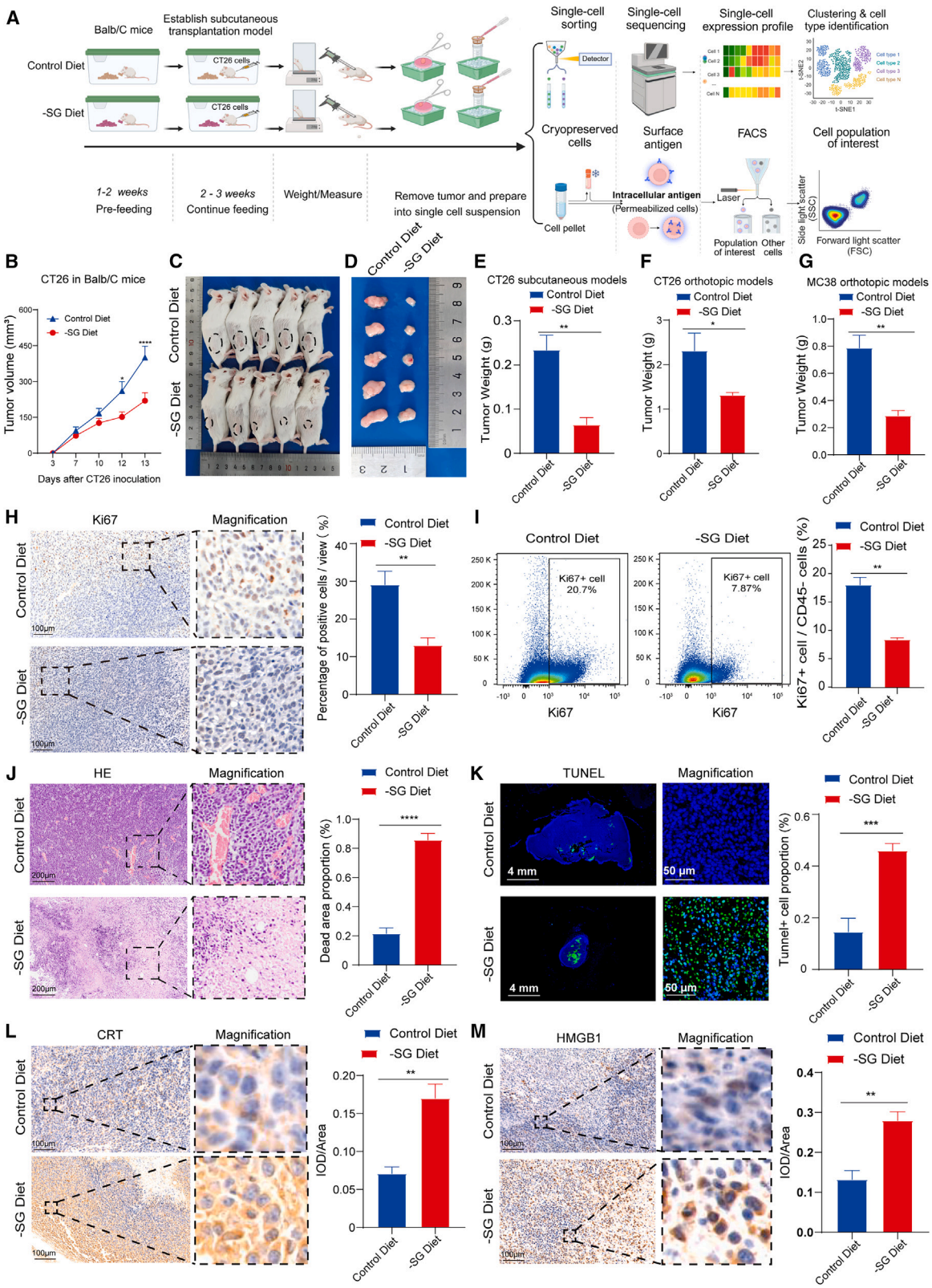

Figure 1. The serine/glycine-free diet restrains colorectal cancer growth and induces immunogenic cell death

(A) Schematic of establishing mouse models with diet serine and glycine restriction and transcriptional characterization.

(B) Tumor volume of CT26 cells in BALB/c mice receiving indicated diets. $n = 22$.

(legend continued on next page)

an immunosuppressive microenvironment.[24–27] The substantial accumulation of lactate stimulates the polarization of tumor-associated macrophages toward an M2 phenotype,[28] inhibits the cytotoxicity of cluster of differentiation 8 (CD8+) T cells and natural killer (NK) cells, reduces the infiltration of cluster of differentiation 4 (CD4+) and CD8+ T cells within the tumor microenvironment (TME),[29,30] and provides metabolic support for tumor-infiltrating regulatory T cells (Tregs).[31] Therefore, it is crucial to undertake in-depth studies into the functions and roles of tumor metabolites, such as lactate, in cancer progression and their impact on the TME. Additionally, investigating how limiting the consumption of external nutrients, including amino acids, affects tumor metabolites, and its implications for antitumor immunity is essential. The potential clinical application of restricting external nutrient intake remains to be further explored.

In this study, we investigated the impact of the serine/glycine-free diet (−SG diet) on tumor and its microenvironment of pMMR/MSS CRC, particularly focusing on the interaction between CD8+ T cells and tumor cells. We first reported programmed death-ligand 1 (PD-L1) lactylation as an underlying mechanism for increased PD-L1 in tumors, contributing to immune evasion and representing a novel target for immunotherapy. Furthermore, we also performed a single-arm, phase I study to evaluate the safety and feasibility of the −SG diet in treating advanced solid tumor. Our findings suggest the −SG diet as a modality in regulating systemic immunity that could be leveraged clinically for cancer treatment.

RESULTS

The –SG diet inhibits CRC growth and promotes tumor cell death

To evaluate the impact of the −SG diet on the proliferation of pMMR/MSS CRC, we performed methyl thiazolyl tetrazolium (MTT) and cell colony formation assays on CT26 cells. These findings demonstrate that the lack of serine and glycine in the medium significantly impeded the proliferation of CT26 cells (Figures S1A and S1B). Besides, EdU assay showed deficiency of amino acids hindered the transition of the cancer cell from G1 to S phase (Figure S1C). Then we investigated the impact of serine and glycine restriction on apoptosis and migration in CT26 cells. Our findings revealed a significant increase in both early and late apoptotic cells (Figure S1D), along with a sharp decrease in migration cells after serine and glycine restriction, compared with CT26 cells cultured in a normal medium (Figure S1E).

We subsequently developed various mouse models to assess potential antitumor effects *in vivo*, including (1) subcutaneous and orthotopic mouse models with CT26 and MC38 cells, (2) a subcutaneous tumor model in nude mice with CT26 cells, (3) a subcutaneous tumor model in recombination activating gene 1 (Rag1) knockout (KO) mice with MC38 cells, and (4) a subcutaneous tumor model with serine transporter SLC12A4 knockdown CT26 cells. All models were treated with both control and −SG diets. Notably, after implementing the −SG diet, the body mass of mice exhibited minimal alteration (Figure S1F). However, the −SG diet significantly impeded tumor growth across various mouse models (Figures 1B–1G and S1G–S1L). In the SLC12A4 knockdown CT26 subcutaneous tumor model, knocking down the SG transporter significantly reduced tumor growth under a control diet. Nevertheless, combining the −SG diet with this knockdown did not confer additional antitumor effects beyond those observed with the −SG diet alone (Figures S1M–S1O). It is noteworthy that the −SG diet decreased the levels of serine and glycine in mice serum (Figure S1P), and we also found the tumor in the −SG diet group exhibited a diminished proliferation capacity through immunohistochemistry (IHC) and flow cytometry (Figures 1H and 1I). The findings from both *in vitro* and *in vivo* experiments offer strong evidence supporting the anti-proliferative effects of the −SG diet in tumors.

Larger necrotic regions and an elevated level of apoptosis were demonstrated in tumors subjected to the −SG diet by hematoxylin and eosin (H&E) and TUNEL staining (Figures 1J and 1K). Moreover, IHC was employed to detect the levels of calreticulin (CRT) and high-mobility group protein box-1 (HMGB1), revealing a significant increase of expression in tumor tissues from the −SG diet group (Figures 1L and 1M). Collectively, these outcomes imply that the observed antitumor effects of the −SG diet in our experimental model are likely to be attributed to immunogenic death rather than alterations in the environment or body weight. Together, these findings suggest that the −SG diet may confer a protective effect against the occurrence and progression of CRC.

The –SG diet modulates intra-tumoral immune milieu

The TME is responsible for adverse prognosis in cancer therapy in some ways,[32,33] and modulating TME to rejuvenate the antitumor immunity[34,35] has become a primary strategy in cancer treatment. The potential of manipulating TME through dietary restriction remains an open question. To address this knowledge gap, we conducted an unbiased analysis of the immune milieu using 10× single-cell RNA sequencing (scRNA-seq) of tumors from both −SG diet and control groups. The cells were classified into 10 major cell types based on graph clustering methods and classical marker annotation (Figures 2A and S2A). Compared with the control group, we observed a significant expansion of lymphocyte clusters, particularly T and B cells, and a reduction in macrophage clusters in tumors (Figures 2B and S2B).

(C and D) Images of BALB/c mice and tumors when harvested. $n = 5$.
(E) Weight of subcutaneous CT26 tumor in BALB/c mice model receiving indicated diets. $n = 5$.
(F) Weight of orthotopic CT26 tumor in BALB/c mice model receiving indicated diets. $n = 5$.
(G) Weight of orthotopic MC38 tumor in C57BL/6 mice model receiving indicated diets. $n = 5$.
(H) Ki67 expression in CT26 subcutaneous tumors evaluated by immunohistochemistry (IHC) staining and quantified. $n = 5$.
(I) Ki67 expression in CT26 tumors evaluated by flow cytometry and quantified. $n = 3$.
(J) Necrotic areas in CT26 tumors were visualized and quantified by H&E staining. $n = 5$.
(K) Apoptosis of CT26 tumors evaluated by TUNEL staining and quantified. $n = 5$.
(L and M) Expression of CRT and HMGB1 evaluated by IHC staining and quantified. $n = 5$.
Data are presented as mean ± SEM, statistically significant by Student's t test. $^{****}p < 0.0001$, $^{**}p < 0.01$.

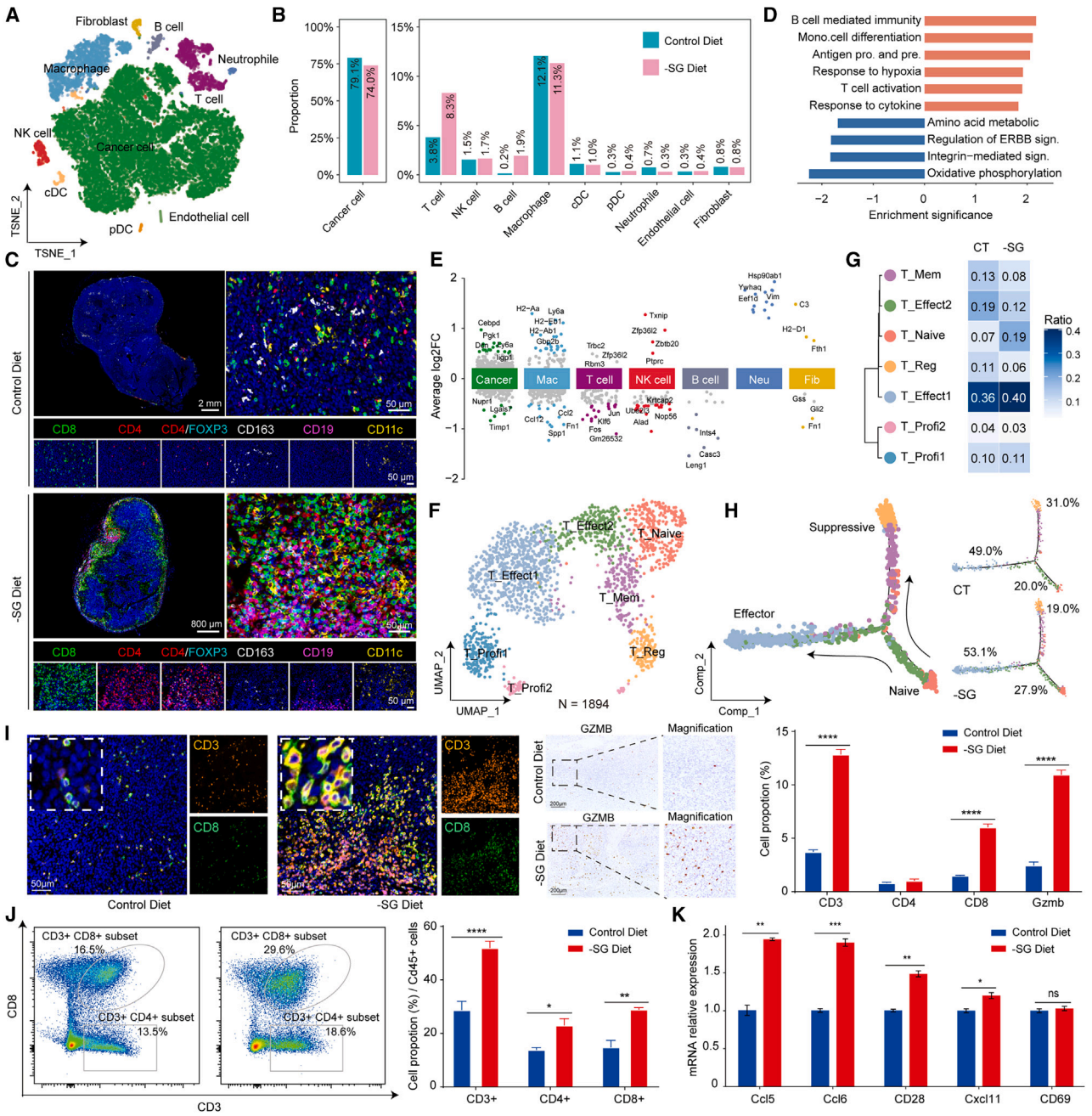

Figure 2. The serine/glycine-free diet modulates the intra-tumoral immune milieu

(A) The t-distributed stochastic neighbor embedding (t-SNE) plot presents all sequenced cells based on cell type.

(B) The bar plot illustrates the proportions of different cell types across various groups.

(C) Infiltration of T cells and B cells in CT26 tumors evaluated by multicolor IHC staining, $n = 4$.

(D) Bar plot shows significantly upregulated (orange) and downregulated (blue) gene sets between two groups as obtained from the GSEA method.

(E) Differential genes for various cell types. The y axis represents the expression fold change after log2transformation, and genes with $\log_2FC > 0.5$ are filled in respective subgroup colors. The top marker genes are annotated in the figure.

(F) Uniform manifold approximation and projection (UMAP) view of T cell clusters.

(G) Dendrogram demonstrating the similarity of T cell cluster centroids. The heatmap shows the proportion of each T cell subset in two groups.

(H) Trajectory analysis shows T cell state transitions in two groups.

(I) Infiltration of CD3+ and CD8+ T cells was visualized by IF staining, and *GZMB* expression was visualized by IHC staining. Quantifications of cell proportion are shown on the right. $n = 5$.

(J) Tumors were assessed by flow cytometry for CD3, CD4, and CD8. Quantifications of cell proportion are shown on the right. $n = 3$.

(K) mRNA expression of *CCL5*, *CCL6*, *CD28*, *CXCL11*, and *CD69* in CT26 tumors cells. $n = 3$.

Data are presented as mean ± SEM, statistically significant by Student's t test. $^{****}p < 0.0001$, $^{**}p < 0.01$, $^{*}p < 0.05$, ns: $p > 0.05$.

CellPress
OPEN ACCESS

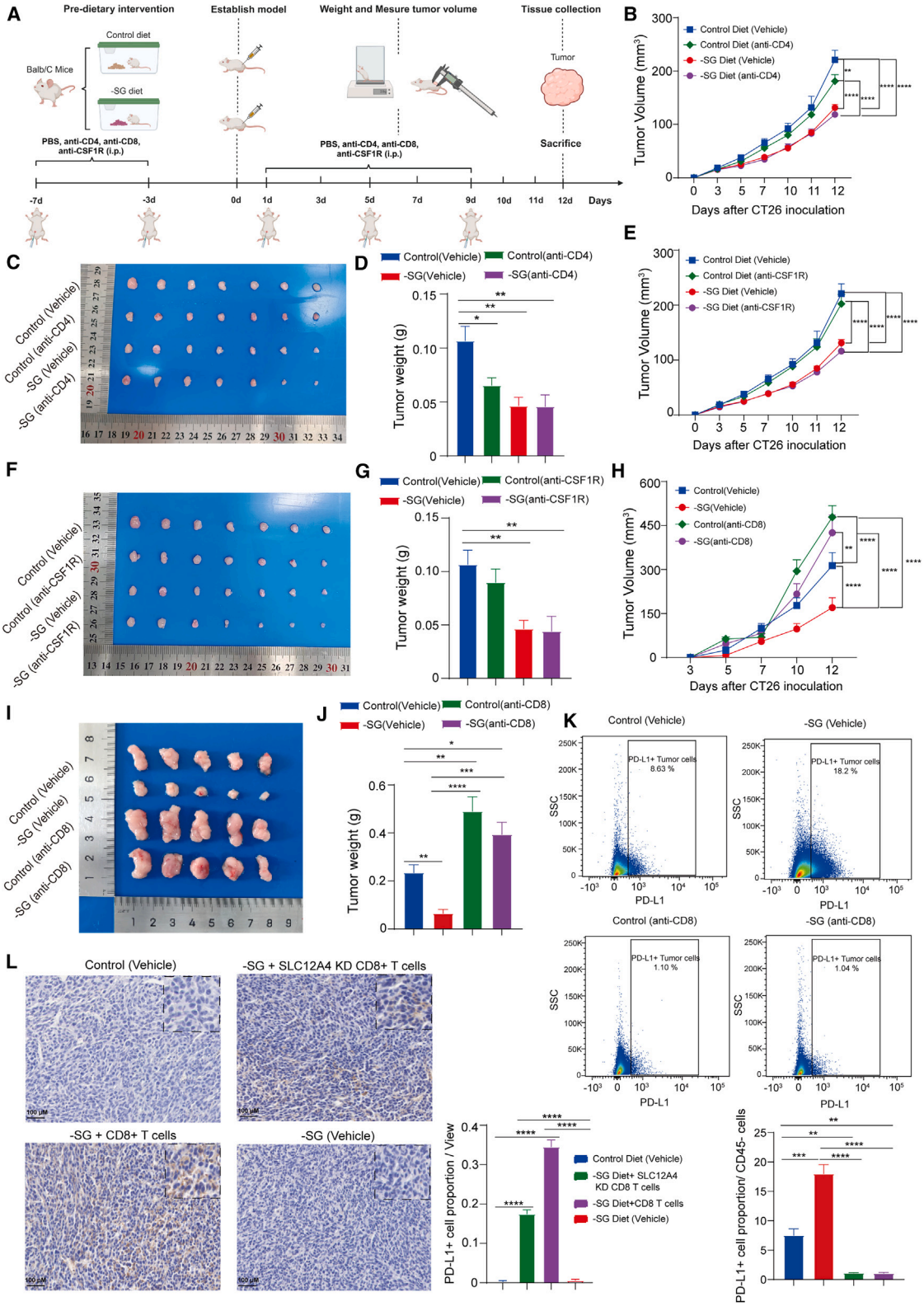

Figure 3. CD8 T cells are required for serine/glycine-free diet-induced reductions in CRC tumor growth

(A) CD4, CD8, or CSF1R antibodies treatment schedule for BALB/c mice bearing subcutaneous CT26 tumors and receiving indicated diets.

(B–D) Tumor volume, images, and weight of subcutaneous CT26 tumors in BALB/c mice receiving CD4 antibody treatments and indicated diets, $n = 7$.

(E–G) Tumor volume, images, and weight of subcutaneous CT26 tumors in BALB/c mice receiving CSF1R antibody treatments and indicated diets, $n = 7$.

(legend continued on next page)

Multicolor IHC further confirmed the substantial infiltration of T cells and B cells in tumors with the −SG diet (Figure 2C). Gene set enrichment analysis (GSEA) of the differentially expressed genes between the two groups revealed a significant upregulation of lymphocyte differentiation and activation, B cell-mediated immunity, and T cell activation pathways (Figure 2D). To evaluate the possible effects of the −SG diet on tumor and immune cells, the differential analysis between these two cell groups indicated that the −SG diet significantly impacted tumor cells, while exerting a relatively minor influence on the functionality of T cells (Figure 2E).

The –SG diet rewires T lymphocytes and diminishes immune-suppressive cells

Subsequently, we conducted separate analyses on the subpopulations of T cells and macrophages, which constituted a substantial proportion. To assess the potential impact of the −SG diet on intra-tumoral T lymphocytes, we performed cluster analysis to clearly distinguish different T cell subpopulations (Figures 2F and S2C). Notably, the significant increase in the proportion of T cells in the −SG diet group was mainly constituted by the sharp rise of naive T cells and effector T cells, while there was a significant decrease in suppressive Tregs (Figures 2G and S2D). The differentiation trajectory of T cells indicated that there was a heightened tendency for T cells to undergo effector-type conversion in tumors of the −SG diet (Figures 2H and S2E). We employed IHC, immunofluorescence (IF), and flow cytometry to further validate the increase of tumor-infiltrating CD8+ T cells in the −SG diet group (Figures 2I, 2J, and S2F). Moreover, we utilized flow cytometry and quantitative real-time PCR (qPCR) techniques to provide additional evidence of the enhanced cytotoxicity and activation phenotype of amplified T cells in tumor tissue from the −SG diet group (Figures 2K, S2G, and S2H). Our findings also revealed that the −SG diet group exhibited a decreased presence of intra-tumoral macrophage subgroup reported to be responsible for suppressing tumor immunity[36–39] (Figures S2I–S2K). These observed changes are believed to contribute to the enhancement of antitumor immunity. Collectively, our data demonstrate that the −SG diet facilitates the transformation of the tumor-infiltrating lymphocytes into effective and cytotoxic phenotypes.

CD8+ T cells are required for –SG diet-induced reductions in CRC tumor growth

Given the substantial alterations observed in CD4+/CD8+ T cells and macrophages, we sought to determine the key cells in this process. We hypothesized that the augmented numbers and phenotypic shifts in CD4+/CD8+ T cells and macrophages might be critical to the antitumor effect under the −SG diet. To investigate our hypothesis, we administered intraperitoneal injections of CD4, CD8, or colony stimulating factor 1 receptor (CSF1R) antibodies to deplete these cells, respectively, in mice on the −SG diet and control group (Figure 3A). No significant changes in tumor size or weight were observed after depleting CD4+ T cells and macrophages (Figures 3B–3G). Remarkably, we observed a significant increase in tumor volume and weight following the depletion of CD8+ T cells, irrespective of whether the treatment included the −SG diet (Figures 3H–3J and S3A). To further determine the antitumor role of CD8+ T cells and the direct antitumor effect of SG-free diet on CD8+ T cells, we magnetically isolated CD8+ T cells and constructed serine transporter SLC12A4 knockdown CD8+ T cells. We then reinfused these cells into the tail vein of nude mice bearing CT26 cells treated with the −SG diet. We found that after reinfusion, the antitumor effect was enhanced compared with the −SG diet alone, further confirming the antitumor activity of CD8+ T cells (Figures S2B–S2E).

In our study, we also observed significant changes in cytotoxic CD8+ T cells whether through the −SG diet or depletion of CD8+ T cells (Figures S2F–S2H). Moreover, we found that the proliferative capability of tumor cells was reduced in the group of the −SG diet. However, the depletion of CD8+ T cells in mice did not have an impact on the proliferation ability of tumor cells (Figure S2I). An intriguing finding was that the level of PD-L1 molecules of tumor cells was significantly reduced after depleting CD8+ T cells in both the −SG diet and control group (Figure 3K). Moreover, we also found that in the absence of CD8+ T cells, PD-L1 expression levels in subcutaneous tumors of both control and −SG-diet-treated nude mice were comparably low. However, following the reinfusion of CD8+ T cells and SLC12A4 KD CD8+ T cells, PD-L1 expression increased significantly (Figure 3L), which suggested the dramatical increased PD-L1 expression along with the exposure to CD8+ T cells. In summary, our data indicate that the protective effect of the −SG diet is contingent upon the presence of CD8+ T cells.

Tumor immunoediting: The battle between CD8+ T cells and tumor cells

Based on the observation that PD-L1 expression on tumor cells vanishes in the absence of CD8+ T cells (Figure 3K), it appears that PD-L1 expression depends on the presence of CD8+ T cells. We then assessed major histocompatibility complex (MHC) class I (MHC class I) molecule expression levels on tumor cells and conducted 10× single-cell T cell receptor sequencing (scTCR-seq) analyses. Initially, we noted an upregulation of MHC class I molecules on tumor surfaces following the −SG diet (Figures S4A–S4D), indicating enhanced antigen-presenting capabilities. Specifically, tumor cells expressing MHC class I molecules can be recognized and attacked by CD8+ T cells via their TCRs.

Subsequently, we analyzed gene proportions in the TCR junction regions (Jα and Jβ) and variable regions (Vα and Vβ) of the −SG group. The proportions of TRAJ-4, TRAJ-13, TRAJ-22, TRAJ-24, TRAJ-26, TRBJ1-5, TRBJ2-1, TRBJ2-2, TRAV3-3, TRAV6-5, TRAV7-3, TRBV2, TRBV10, TRBV19, and TRBV31 were elevated compared with the control group, suggesting increased TCR diversity and antigen specificity (Figures 4A–4C). Further examination revealed specific patterns in the correlations between V and J segment usage within the TCRα and

(H–J) Tumor volume, images, and weight of subcutaneous CT26 tumors in BALB/c mice receiving CD8 antibody treatments and indicated diets, $n = 5$.
(K) Tumor were assessed by flow cytometry for PD-L1, $n = 3$.
(L) Tumor of BALB/c nude mice were assessed by IHC for PD-L1, $n = 5$.
Data are presented as mean ± SEM, statistical significance by ANOVA followed by Student's t test. $^{****}p < 0.0001$, $^{***}p < 0.001$, $^{**}p < 0.01$, $^{*}p < 0.05$.

CellPress
OPEN ACCESS

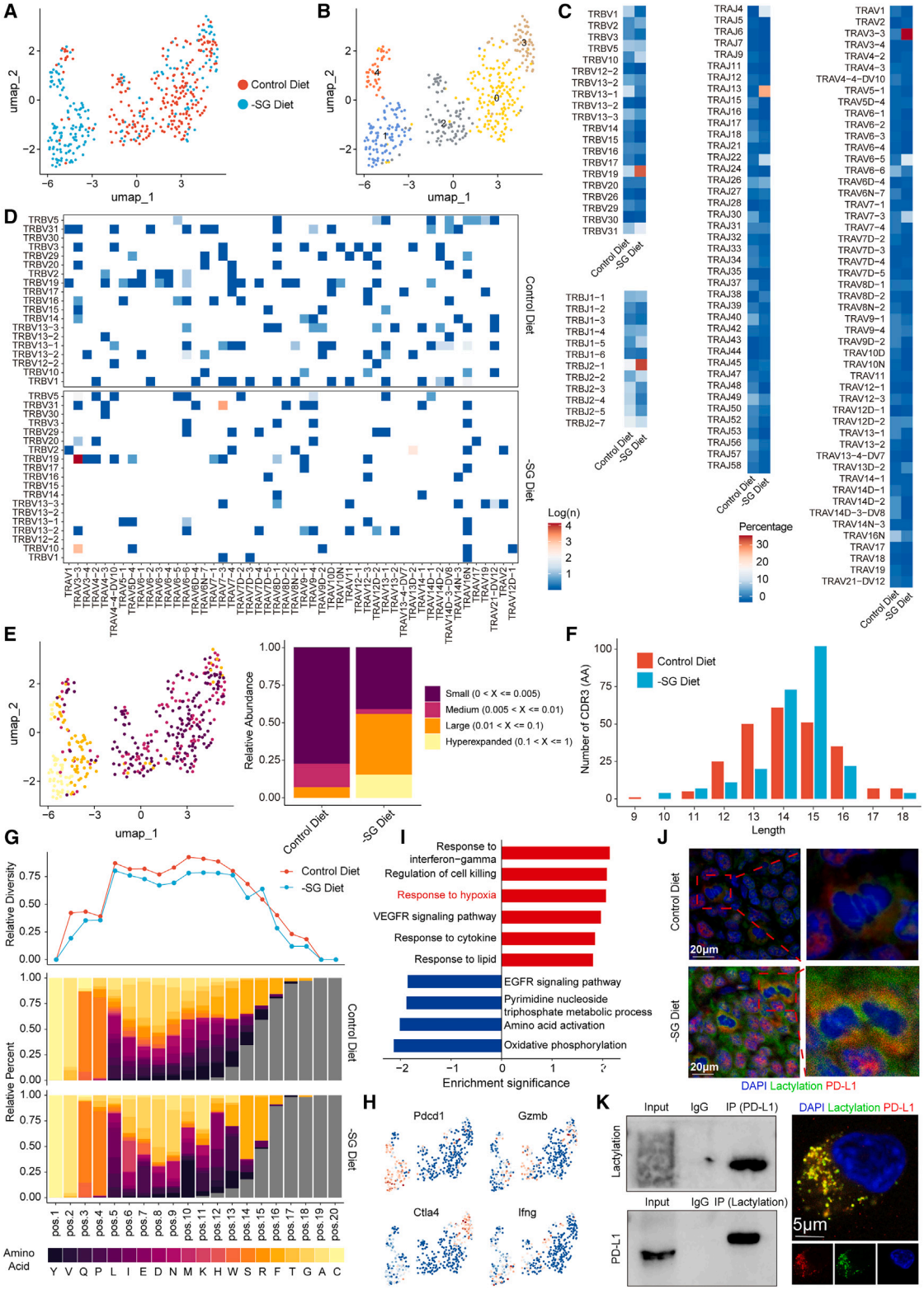

Figure 4. The alteration of TCR diversity in T cells after the serine/glycine-free diet

(A) The UMAP plot presents T cells from control and −SG diet.

(B) The graph-based clustering results of T cells in UMAP plot.

(C) The heatmap shows percentage of each TCR from control and −SG diet group.

(legend continued on next page)

TCRβ chains (Vα-Jα, Vβ-Jβ) and across TCRαβ chains (Vα-Vβ, Vα-Jβ, and Vβ-Jα) (Figure 4D). Additionally, we observed large and hyper-clonal TCR expansion in the −SG diet group (Figure 4E). The third complementarity determining region 3 (CDR3) is vital for the diversity of TCRs.[34,35,39] Our analysis of CDR3 sequence length revealed a predominance of sequences 14 and 15 amino acids long in the −SG diet group, indicating an enhanced ability to recognize various antigens due to increased amino acid site diversity (Figure 4F). Significant differences in amino acid preferences between the sequences of both groups were also noted (Figure 4G). Taken together, these results highlight the augmented TCR diversity and antigen specificity in the −SG diet group, indicative of a robust epitope-specific T cell response.

However, during the interaction between tumors and CD8+ T cells, tumor cells can mutate to evade immune cell killing and achieve immune escape by upregulating immune checkpoint molecules and inducing PD-1 expression in T cells. We noted that hyper-expanded T cell subsets in the −SG diet group exhibited high PD-1 expression (Figure 4H), suggesting the necessity to inhibit the PD-1/PD-L1 pathway to enhance T cell functionality and antitumor immunity. Further investigation into immune checkpoint interactions revealed a notable increase in PD-L1 engagement in the −SG diet group, whereas interactions with other immune checkpoints remained consistent (Figure S4E). These results partially confirm the causal link between CD8+ T cell activity and increased PD-L1 expression on tumor cells in a SG-deficient diet.

Next, we tested the levels of PD-L1 expression and found a significant increase in PD-L1 protein without an obvious change in mRNA in tumor cells (Figures S4F–S4H). To investigate the mechanism behind this, we conducted a comprehensive analysis of PD-L1 degradation. Our next study was promoted by the results of a GSEA of differential expressed genes which indicated an increased tumor cell response to hypoxia and improved regulation of cell killing (Figures 4I and S4I–S4L). It is worth noting that hypoxic conditions lead to the production of lactic acid, which may be uptaken via lactate transport monocarboxylate transporters (MCTs) to promote lactylation modifications on proteins.[36–38,40] Therefore, our results from IHC indicated a general increase in lactylation levels of tumor in the −SG diet (Figure S4M). However, the lactylation of PD-L1 and its specific role are currently unknown. Subsequently, we conducted multicolor IHC and found that the lactylation levels of tumor PD-L1 were significantly increased in the group with the −SG diet (Figure 4J). We also observed that PD-L1 interacted with lactylation, as evidenced by the impeded co-immunoprecipitation (coIP) and IF staining (Figure 4K).

PD-L1 lactylation contributes to delaying tumor PD-L1 degradation

To further investigate the mechanism of PD-L1 lactylation and its impact on tumor cells, we utilized western blotting to assess levels of hypoxia-inducible factor-1 alpha (HIF-1α), glycolytic enzymes hexokinase 1 (HK1), pyruvate kinase M2 (PKM2), and lactate dehydrogenase A (LDHA), PD-L1 acyltransferase general control non-depressible 5 (GCN5), and deacyltransferase sirtuin 5 (SIRT5) in tumors. Additionally, we analyzed tumor homogenates and serum from CT26 tumor cell-bearing mice using targeted organic acid metabolomics. PD-L1 was selectively enriched through immunoprecipitation, and specific lactylation sites were identified via mass spectrometry (MS). The results indicate that the −SG diet activates HIF-1α, thereby enhancing glycolysis in tumors (Figures 5A and S5A), which in turn raises lactate levels (Figure 5B) and promotes the high expression of the acyltransferase GCN5 (Figures 5C and S5B). This leads to the lactylation of lysine encoded by the PD-L1 DNA sequence 810–813 (Figures 5D and S5C). To assess the antitumor effects of PD-L1 lactylation, we mutated the lactylation sites of the PD-L1 protein from lysine to glutamate and knocked down PD-L1 in another group. The results indicated that both knocking down PD-L1 and mutating the PD-L1 lactylation sites in tumor cells exhibited antitumor effects, with the mutation group showing weaker antitumor activity compared with direct PD-L1 knockdown (Figures 5E–5G and S5D–S5F). This suggests that PD-L1 lactylation is a negative regulatory mechanism promoting tumor immune evasion. Furthermore, to assess the clinical applicability of PD-L1 lactylation and validate the association between PD-L1 lactylation and cellular glycolysis, we utilized tissue microarrays from CRC patients along with multiplex IHC techniques. We discovered a positive correlation between the level of glycolysis and overall tumor lactylation. Additionally, the degree of lactylation in the entire tumor tissue correlates positively with both the lactylation level and expression level of PD-L1, further confirming the positive correlation between PD-L1 lactylation and its expression (Figures 5H and 5I).

To elucidate the specific role of PD-L1 lactylation, CT26 cells were treated with BAY-8002 to increase cellular lactate levels, and with 2-hydroxyglutarate (2-HG, a pyruvate dehydrogenase [PDH] inhibitor) and FX11 (an LDHA inhibitor) to inhibit lactate production. We found that the expression of PD-L1 underwent a dose-dependent and time-dependent alteration (Figure 5G). The effects of BAY-8002, 2-HG, and FX11 on PD-L1 expression were also validated through IF staining (Figure 5K). The cycloheximide chase assay (CHX)[41] revealed that FX11 and 2-HG hindered PD-L1 lactylation and accelerated its the degradation. In contrast, BAY-8002 primarily stabilized or even enhanced the expression level of PD-L1 (Figure 5L). Consequently, it can be

(D) The heatmap shows the matching patterns of TCRA and TCRB in control and −SG diet group.
(E) The results of T cells with different clonal expansion characteristics, exhibiting the distribution in UMAP plot and the proportions from control and −SG diet group in bar plot.
(F) The distributions of the length in CDR3 amino acid sequence from control and −SG diet group.
(G) The preference of the amino acid composition in CDR3 from control and −SG diet group.
(H) The expression of Pd-1, Gzmb, Ctla4, and Ifng in T cells.
(I) Bar plot shows significantly upregulated (red) and downregulated (blue) gene sets in cancer cells as obtained from the GSEA method.
(J) Lactylation of PD-L1 tested by bicolor IHC staining. Lactylation (green), PD-L1 (red), and DAPI (blue). Scale bar, 10 μm, $n = 5$.
(K) The interaction between PD-L1 and lactic acidification detected by co-immunoprecipitation and immunofluorescence, $n = 3$.

CellPress
OPEN ACCESS

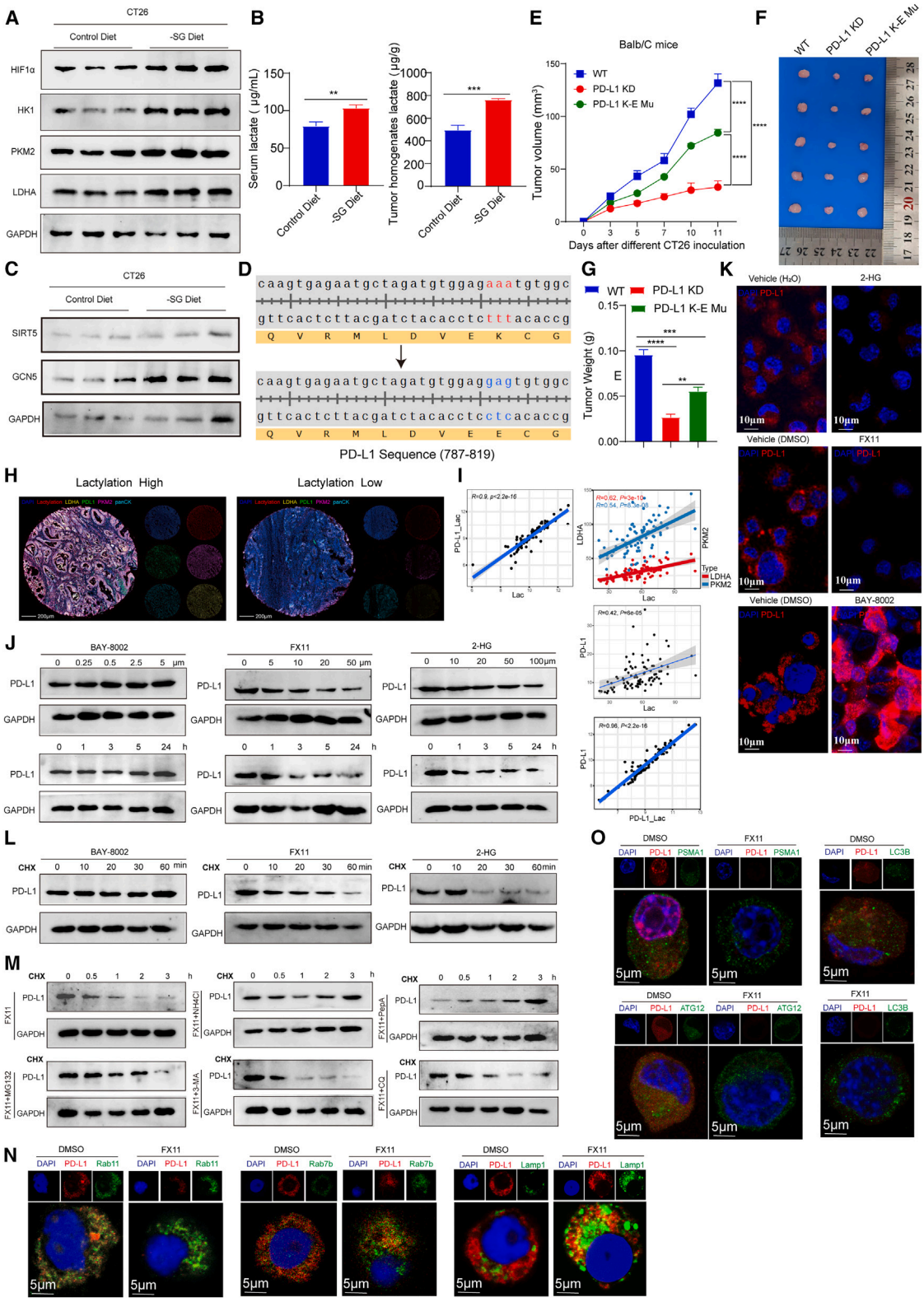

Figure 5. PD-L1 lactylation contributes to delaying tumor PD-L1 degradation

(A) Western blot analysis of HIF-1α, glycolysis enzymes (HK1, PKM2, and LDHA) expression in CT26 tumor mice model treated with indicated diets.

(B) Lactate level in tumor-bearing mice serum and tumor homogenates, $n = 5$.

(C) Western blot analysis of PD-L1 acyltransferases GCN5, and deacylases SIRT5 expression in CT26 tumor mice model treated with indicated diets.

(legend continued on next page)

inferred that lactylation of PD-L1 protein has the potential to stabilize the protein and prevent its degradation.

To investigate protein degradation pathways involved, we employed lysosomal inhibitors NH_4Cl and pepstatin A (PepA), proteasome inhibitor MG132, and autophagy inhibitors 3-methyladenine (3-MA) and chloroquine (CQ). Our findings revealed that lysosomal inhibitors NH_4Cl and PepA could counteract the inhibitory effect of FX11 and 2-HG on lactylation, leading to an enhanced degradation of PD-L1. However, the proteasome inhibitor MG132 and the autophagy inhibitors 3-MA and CQ were unable to reverse the inhibitory effects (Figures 5M and S5G). To confirm the role of those cell components in PD-L1 degradation and investigate the impact of lactylation on PD-L1 trafficking, we inhibited PD-L1 lactylation and examined its distribution in different subcellular organelles. As anticipated, treatment with FX11 and 2-HG significantly decreased the co-localization of PD-L1 with Rab11-labeled recycling endosomes while increased the co-localization of PD-L1 with Rab7b-labeled late endosomes and lysosomal-associated membrane protein 1 (Lamp1)-labeled lysosomes (Figures 5N and S5H), while there was minor difference in the co-localization of PD-L1 with proteasome subunit alpha type-1 (PSMA1)-labeled proteasome, autophagy-related 12 (ATG12), and microtubule-associated protein 1 light chain 3 beta (LC3B)-labeled autophagosome (Figures 5O and S5I). In short, these consistent results indicate that lactylation of PD-L1 prevents its degradation through the lysosomal pathway.

The –SG diet sensitizes CRC to α-PD-1 in mice model

It has been reported that increased T cell infiltration, particularly involving interferon-γ (IFN-γ), may explain why d-MMR/MSI-H CRC respond more favorably to immunotherapy compared with pMMR/MSS CRC.[42,43] Consequently, modulating the TME of pMMR/MSS CRC could potentially enhance the efficacy of ICIs. In our study, we found that the −SG diet significantly increased CD3+ and CD8+ T cell infiltration, as well as IFN-γ and PD-L1 levels in pMMR/MSS CRC. This led us to investigate whether blocking the interaction between PD-L1 on tumor cells and PD-1 on T cells could amplify the antitumor effect. To explore the potential impact of the −SG diet on the responsiveness of pMMR/MSS CRC to PD-1 inhibitors, we established various subcutaneous and orthotopic tumor models (Figure 6A). Our results showed that treatment with anti-PD-1 alone had a minimal effect on the volume of pMMR/MSS CRC but was significantly more effective in d-MMR/MSI-H CRC. However, combining the −SG diet with PD-1 inhibitors resulted in enhanced inhibition of tumor growth and a significant reduction in tumor weight (Figures 6B–6D and S6A–S6G).

Importantly, the combination of the −SG diet with anti-PD-1 treatment significantly increased the presence of CD3+ and CD8+ T cells (Figure 6E). Anti-PD-1 therapy notably improved the proliferation of CD4+ and CD8+ T cells in the control group. However, in the −SG diet group, the proliferation of CD4+ T cells was modestly enhanced following PD-1 inhibitor administration, with no significant change in CD8+ T cell proliferation compared with the group receiving only the −SG diet (Figure 6F). Furthermore, our study revealed that combining the control group with anti-PD-1 therapy significantly reduced tumor cell proliferation. Yet, there was no notable difference in tumor cell proliferation when comparing the −SG diet group with the combination of the −SG diet and anti-PD-1 therapy (Figure S6H). The use of anti-PD-1 also increased the expression level of PD-L1 on tumor cell surfaces (Figure 6G). Additionally, we conducted further tests to assess macrophage expression levels; we observed an increase in MHC class II and a decrease in secreted phosphoprotein 1 (SPP1) expression in macrophages (Figures 6H and 6I), suggesting enhanced antigen presentation and reduced inhibitory immune function, respectively. Overall, these findings indicate that the −SG diet may enhance the sensitivity of refractory pMMR/MSS CRC tumors to anti-PD-1 therapy.

The –SG diet is feasible and safe for advanced solid tumor patients in a single-arm, phase I study

Following the promising results of our preclinical studies, we initiated a single-arm, phase I clinical trial on the −SG diet for patients with advanced solid tumors. This trial was approved by the Ethics Committee on Biomedical Research of West China Hospital, Sichuan Provincial People's Hospital and Xinjin District Hospital of Traditional Chinese Medicine and was registered in the Chinese Clinical Trial Register (ChiCTR2300067929). The

(D) PD-L1 DNA sequence mutation (810–813, lysine to glutamic acid).
(E–G) Tumor volume, images, and weight of BALB/c mice subcutaneously incubated CT26 cells, CT26 cells knocking down PD-L1, and CT26 cells receiving PD-L1 mutation respectively, $n = 5$.
(H) The degree of tumor lactylation, the expression of LDHA, PD-L1, and pan-cytokeratin (PanCK) in tissue microarrays from colorectal patients, evaluated by multicolor IHC staining.
(I) Correlation analysis of lactylation modification and PD-L1 lactylation, lactylation modification and glycolytic enzymes (LDHA and PKM2), lactylation modification and PD-L1 expression, and PD-L1 lactylation and PD-L1 expression.
(J) Western blot analysis of PD-L1 expression in CT26 cells treated with 2-HG, FX11, or BAY-8002 in a dose-dependent and time-dependent manner.
(K) PD-L1 expression of CT26 treated with 2-HG, FX11, or BAY-8002 for 24 h and then evaluated by IF staining. PD-L1 (red) and DAPI (blue). Scale bar, 10 μm, $n = 3$.
(L) CT26 cells were pretreated with BAY-8002, FX11, and 2-HG for indicated time points, then incubated with cycloheximide for 2 h. The levels of PD-L1 were detected by western blot.
(M) Western blot analysis of PD-L1 expression in CT26 cells treated with FX11 and lysosomal inhibitors NH_4Cl, pepstatin A, proteasome inhibitor MG132, autophagy inhibitors 3-MA or CQ.
(N) Colocalization of PD-L1 with Rab11, Rab7b, or Lamp1 by IF staining with Rab11, Rab7b, and Lamp1 (green), PD-L1 (red), and DAPI (blue) after 24h treatment of lactylation inhibitor FX11.
(O) Colocalization of PD-L1 with PSMA1, ATG12, or LC3B by IF staining with PSMA1, ATG12, and LC3B (green), PD-L1 (red), and DAPI (blue) after 24h treatment of lactylation inhibitor FX11.
Data are presented as mean ± SEM, statistically significant by Student's t test. $^{***}p < 0.001$, $^{**}p < 0.01$.

CellPress
OPEN ACCESS

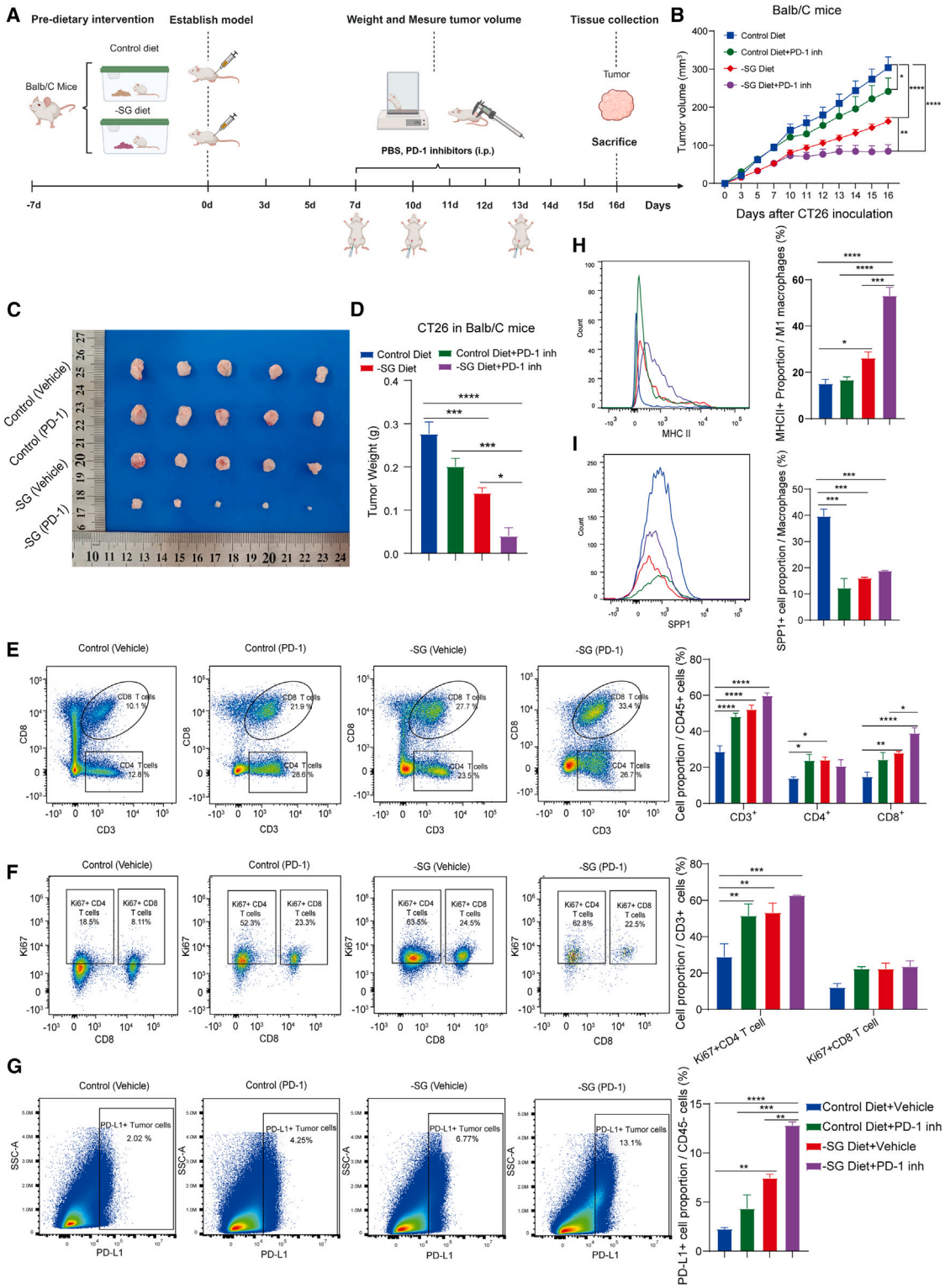

Figure 6. The serine/glycine-free diet sensitizes CRC to α-PD-1 treatment in mice model

(A) PD-1 inhibitors treatment schedule for BALB/c mice bearing subcutaneous CT26 tumors.

(B) Tumor volume of BALB/c subcutaneous CT26 tumor mice model receiving indicated treatments. *n* = 10.

(C) Images of CT26 tumors when harvested. *n* = 5.

(D) Tumor weight of CT26 cells in BALB/c mice receiving indicated treatments. *n* = 5.

(legend continued on next page)

primary outcome of this trial was to evaluate the safety of the −SG diet and the serum amino acid metabolism levels in patients. Secondary outcomes included assessing patient tolerability and the potential antitumor effects, such as in tumor size reduction and changes in blood immune cell levels. Eligible patients were enrolled and registered at three hospitals in China, serving as the trial sites. Informed consent was obtained from all participants or their legal guardians. The detailed inclusion and exclusion criteria were described in STAR Methods.

Between March 2022 and September 2023, a total of 28 patients with advanced solid tumor were assessed for eligibility and 20 patients were enrolled in the single-arm trial. Specific clinical study design and patient disposition were shown in Figures S7A and S7B. During the trial, five patients withdrew midway because they could not adapt to a daily diet consisting solely of nutritional powders or other low-serine and glycine foods. Ultimately, 20 patients completed at least one cycle of the −SG diet and were included in the subsequent analysis. The average age of the patients included in the analysis was 66 years (range, 52–70 years), with no gender bias (p = 0.2632), and 7 (35%) were women. Among these patients, 10 (50%) were diagnosed with CRC, 4 (20%) were diagnosed with lung cancer, 3 (15%) were diagnosed with esophageal cancer, 2 (10%) were diagnosed with gastric cancer, and 1 (5%) were diagnosed with hepatoma. The International Tumor, Node, Metastasis (TNM) staging system were III and IV (n = 4 in stage III and n = 16 in stage IV). Detailed patient information was summarized in Table S1.

In this interim data analysis, we analyzed the adverse events (AEs) associated with the −SG diet. The predominant AE observed was gastrointestinal toxicity, with grade 1 or 2 toxicities, including nausea, flatulence, and diarrhea, being prevalent. Of the included patients, 65% experienced diarrhea, 25% reported nausea, and 20% suffered from flatulence (Figure 7A), which were all effectively managed with routine symptomatic treatments (Figure 7B). No unexpected toxicities were noted during the trial, and all adverse reactions were managed according to established guidelines. Detailed information about the AEs and their severity is presented in Table S2. Importantly, physiological parameters such as blood routine and liver and kidney functions remained unchanged after the completion of the −SG diet in each cycle, shown in Table S3. Similarly, there were no significant changes in the body mass index (BMI) of patients, which corresponds to results observed in mouse models (Figure 7C). Furthermore, the quality of life for over 90% of the enrolled patients was not impacted (Figure 7D). Overall, our findings suggest that the −SG diet is feasible and safe for humans with advanced solid tumors.

Correlation of the –SG diet with clinical responses, metabolism, and immunity

Among the 20 patients who received the −SG diet, 5 patients (5 of 20, 25%) achieved a partial response (PR), 13 patients (13 of 20, 65%) had a stable disease (SD), and 2 patients (2 of 20, 10%) achieved a progressive disease (PD) (Figures 7E and 7F). Overall response rate (ORR) was 25%, clinical benefit rate (CBR) was 90%. Significant clinical responses in patients treated with the −SG diet are evident in computed tomograph (CT) scans (Figure 7G) and endoscopies (Figure 7H). Next, we also evaluated the potential efficiency of the −SG diet, and we observed a significant reduction in serum serine and glycine levels in patients who received the −SG diet (Figure 7I). To gain further insight into the effectiveness of the −SG diet in regulating immunity, we conducted flow cytometry analysis of peripheral blood mononuclear cells (PBMCs). Our results revealed that the expression levels of granzyme B (GZMB) and IFN-γ in both CD4+ and CD8+ T cells significantly increased after the treatment of the −SG diet (Figures 7J and 7K). Finally, we investigated the relationship between serum serine levels, immune T cells, and tumor clinical responses, identifying a potential correlation among them (Figure 7L). In all, our results provide a potential dietary strategy for advanced solid tumors.

DISCUSSION

Collectively, we have provided substantial evidence that the −SG diet impacts both tumor cells and CD8+ T cells. This diet significantly lowers the levels of serine and glycine in the blood, impeding their absorption by tumor cells, which in turn inhibits tumor growth. Furthermore, it induces tumor cells to release chemotactic factors such as C-C motif chemokine ligand 5 (CCL5) and C-X-C motif chemokine ligand 11 (CXCL11), recruiting CD8+ T cells to the tumor sites. Once these T cells recognize MHC class I molecules on the tumor surface via their TCR, they are activated and transform into a more cytotoxic phenotype, thereby enhancing their tumor-targeting capabilities. However, tumor cells may stabilize PD-L1 expression through lactylation, thereby reducing the efficacy of CD8+ T cells. Consequently, inhibiting the PD-1/PD-L1 pathway can restore the functionality of CD8+ T cells and enhance the antitumor response. Additionally, we have conducted a phase I clinical trial that preliminarily confirms the feasibility, safety, and potential efficacy of the −SG diet. In summary, all our findings suggest a potential strategy of combining the −SG diet with immunotherapy.

Many cancers rely on various amino acids, including serine and glycine, to support their development.[15,16,19,21,23,44–46] Consequently, restricting amino acid intake, particularly through dietary modulation, has emerged as a potential strategy to curtail tumor growth and shows promising prospects in cancer treatment. Our research has demonstrated the effectiveness of the −SG diet in inhibiting tumor growth and promoting tumor cell death. This research not only confirms earlier studies on the −SG diet, which primarily focused on the tumor itself rather than the TME, but also expands on these findings. We have shown that reduced SG intake can impair tumor growth and,

(E–G) Tumors were assessed by flow cytometry for CD3/CD4/CD8 (E), Ki67 on CD4+ and CD8+ T cells (F), and PD-L1 expression of tumor cells (G), n = 3.
(H and I) MHC class II (H) and SPP1 (I) expression of macrophage in tumor single-cell suspension detected by flow cytometry, n = 3. Quantifications of cell proportion are shown on the right.
Data are presented as mean ± SEM, statistical significance by ANOVA followed by Student's t test. ****p < 0.0001, ***p < 0.001, **p < 0.01, *p < 0.05.

CellPress
OPEN ACCESS

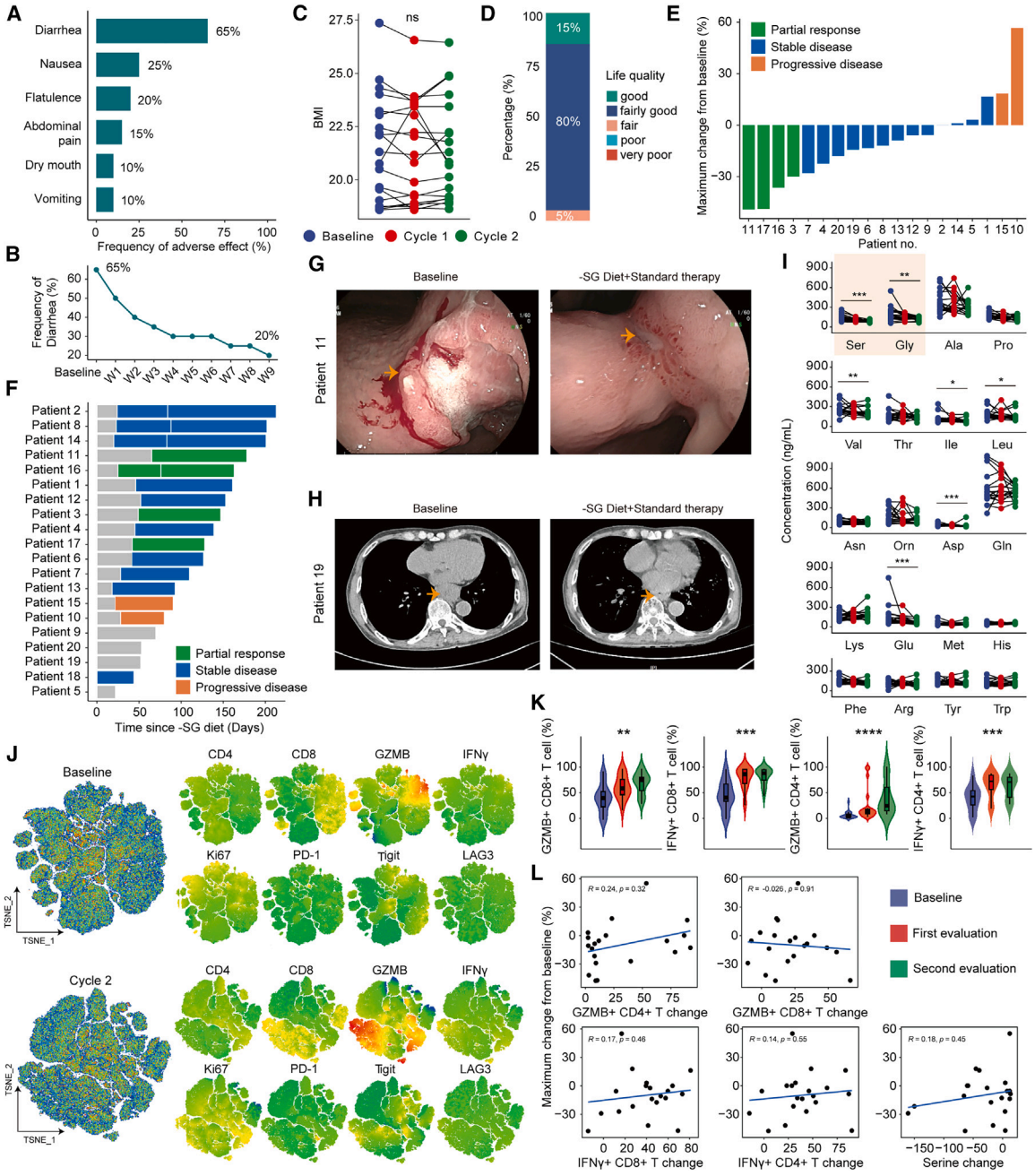

Figure 7. Exploring the clinical application potency of the serine/glycine-free diet

(A) Frequency of adverse reactions.

(B) The lasting time of diarrhea.

(C) BMI of patients pre- and post-diet treatment.

(D) Quality of life assessment in patients receiving an amino-acid-deficient diet.

(E) Waterfall plot of the maximum change in the sum of the target lesion compared with baseline measurements in 20 patients.

(F) Swimmer plots of the change in the sum of the target lesions from the treatment in 20 patients.

(G) Endoscopies of patient 11 treated with the −SG diet.

(H) CT scans of patient 4 treated with the −SG diet.

(I) Serum amino acid concentration of CRC patients pre- and post-diet treatment.

(J) The t-SNE plot presents patients' peripheral blood samples collected at baseline and after 2 cycles of diet treatment were assessed by flow cytometry.

(K) Patients' peripheral blood samples collected at baseline and after 1 and 2 cycle of diet treatment were assessed by flow cytometry for GZMB, IFN-γ on CD4+ and CD8+ T cells.

(L) The correlation between changes in patients' immune cells, serum level, and tumor size.

by altering the TME, can enhance T cell infiltration and cytotoxicity in CRC. Therefore, we believe that the increased infiltration and phenotypic shift of T cells in CRC, induced by the −SG diet, could be beneficial in improving the response of tumors.

Contrary to most of previous studies[47,48] and our own *in vitro* results, we observed that the −SG diet significantly promotes the activation and proliferation of CD8+ T cells *in vivo*. First, we analyzed the differences between previous studies and our *in vivo* data, which may be attributed to variations in animal models and tissue sampling sites. Previous research found that the −SG diet inhibited the T cell response to listeria monocytogenes expressing ovalbumin (LmOVA) infection *in vivo*, significantly reducing the percentage and number of ovalbumin (OVA)-specific CD8+ CD45.2+ T cells in the spleen.[47] This may explain why our observations within the tumor are contrary to these findings. Then, to further explore the reasons for the stark differences between *in vivo* and *in vitro* behaviors of CD8+ T cells, we noted an increase in the secretion of chemotactic factors CCL5 and CXCL11 by tumor cells, which facilitates the recruitment of CD8+ T cells into the tumor tissue.[49–51] Subsequently, we conducted a detailed analysis of MHC class I molecule expression on tumor cells and characterized the TCR features on T cells. We found that elevated expression of MHC class I molecules on tumor cells enhances TCR recognition, thereby increasing their tumor-targeting efficacy.[52–55] Additionally, the −SG diet significantly increased the clonotype diversity and antigen specificity of CD8+ T cells. Therefore, we believe that activation through TCR engagement and interaction with co-stimulatory molecules triggers a transition from naive T cells to an anabolic state, promoting extensive T cell proliferation and intensifying their assault on tumor cells.[56–60] Furthermore, it is reported that lactate increases stemness of CD8+ T cells to augment antitumor immunity.[61] In our study, we demonstrated that the lactate level in tumor tissue increased in the −SG diet group. This increase may also enhance the stemness of CD8+ T cells, thereby promoting their proliferation.

Despite its impact on lymphocytes, the −SG diet has also demonstrated to increase the protein level of PD-L1 without significant alterations in its mRNA levels. Moreover, we have also identified a novel PD-L1 modification called lactylation mediated by lactyltransferases GCN5. This process utilizes the excessive lactate from the enhanced glycolysis induced by the −SG diet through the activation of HIF-α under hypoxia conditions. Several post-translational modifications (PTMs) of PD-L1, such as glycosylation, palmitoylation, and deubiquitylation, have been proven to contribute to its stabilization.[62–69] Previous studies have shown that PD-L1 subjected to such modifications can be stabilized or degraded by cellular components like lysosomes,[70–75] proteasomes[76,77] and autophagosomes.[78–80] Besides, glycosylation of PD-L1 can establish an immunosuppressive TME,[65,69] and deubiquitylation can inhibit tumor immunogenicity.[62,64] Furthermore, current research on protein lactylation predominantly centers on histones, aimed at regulating tumor progression from an epigenetic perspective.[36,40,81–84] However, the understanding of lactylation's impact on non-histone proteins, particularly in terms of investigating tumor progression through lactylation at the protein and PTM levels, remains limited. To our knowledge, we first reported that the PD-L1 lactylation has exhibited an important role in increasing PD-L1 protein level in tumor cells and promoting immune evasion. The tumor cells show a great tendency to use lactate to modify PD-L1 in response to the recruited cytotoxic T cells by the −SG diet, preventing PD-L1 degradation in lysosomes and thus stabilizing its protein level. The interplays between immune responses and the alterations of metabolites levels induced by the −SG diet indicate a possible approach to modulate TME and tumor immunogenicity by manipulating tumor metabolism. The accumulated PD-L1 resulting from lactylation could also be seen as a significant target for anti-PD-1 therapy. Specifically, due to the PD-L1 increase on the surface of tumor cells, triggered by the −SG diet, there is an initiation of immune escape. Consequently, inhibiting the interaction between T cell PD-1 and tumor cell PD-L1 can significantly enhance antitumor immunity. Collectively, our research opens up a potential strategy for combining the −SG diet with immunotherapy for solid tumor.

Based on the results obtained from the mouse model, we aimed to translate this research into clinical practice to benefit a broader range of tumor patients. Consequently, we conducted a phase I, single-arm clinical trial on the effect of the −SG diet. Our primary outcome is the safety and feasibility of the −SG diet in cancer patients. Our findings revealed that patients who received the −SG diet exhibited various slight gastrointestinal symptoms with 1 or 2 grade severity, predominantly diarrhea, which could be manageable by routine treatment. In addition, those gastrointestinal symptoms have minimal influence on the patients' body weight and quality of life. It is hypothesized that the adverse effects could be attributed to the heterogeneity among patients, such as the difference of intestinal sensitivity or adaptation. Additionally, the external factors, including inadequate dietary fiber and probiotics intake,[85–88] may also contribute to diarrhea. In general, this regimen has a high degree of safety with minor adverse effects. In the future, it is considerable to increase the proportion of dietary fiber and probiotics supplementation in the current diet powder formulations to alleviate the discomfort of the patients.

The amino acids level in serum could be altered by the −SG diet, which has been proven in mouse models. We are the first to discover that the −SG diet could disrupt the homeostasis of systemic amino acids with durable influence on patients with advanced solid tumor in clinical practice. We also observed a notable elevation in the proportions of GZMB and IFN-γ of systemic CD4+ and CD8+ T cells in peripheral blood from patients enrolled in the clinical trial, which corroborates our finding from mouse models. Moreover, we identified a potential correlation among serum serine levels, immune T cells, and clinical responses in tumors. This indicates that the −SG diet could potentially enhance systemic immunity and provide a theoretical foundation for tumor therapy. Our research may bring insights into the treatment strategy not only in tumor but also in a wider range of metabolism-related disorders. Ultimately, further clinical trial in larger cohorts is imperative, and the application of this approach opens up a promising adjuvant strategy in solid tumor therapy.

Limitations of the study

There are several limitations to our study. From the perspective of clinical application, further refinement of the dietary proportions of the dietary powder, such as increasing the proportion of dietary fiber, probiotics, is required to achieve a more balanced dietary components for patients. Additionally, improvement

in the taste of dietary powders is also necessary to better align with patients' preferences. Given that our clinical trial was a phase I study focusing primarily on the safety of the −SG diet, we did not delve deeply into efficacy issues. Considering the limited number of patients in current research, future clinical trials are also required to further confirm the effectiveness of the −SG diet, and its combination with immunotherapy in the larger population. Furthermore, the genetic variability among the patient cohort was not extensively explored in this study, which may limit the generalizability of our findings. Future studies should include a more genetically diverse patient population to assess the potential variability in response to the −SG diet. Addressing these limitations will be crucial in future research to enhance the robustness and applicability of our findings.

RESOURCE AVAILABILITY

Lead contact

Further information and requests for resources and reagents should be directed and will be fulfilled by the lead contact, Dr. Xuelei Ma (drmaxuelei@gmail.com).

Materials availability

This study did not generate new unique reagents.

Data and code availability

- Uncropped western blots and source data can be found in Data S1.
- This clinical trial protocol could be found in the supplemental information.
- The original data for visualizing scRNA-seq and scTCR-seq are on GEO and are publicly available as of September 16, 2024.
- This paper does not report original code.
- Any additional information required to reanalyze the data reported in this paper is available from the lead contact upon request.

ACKNOWLEDGMENTS

This study was supported by grants from the Science and Technology Program of Sichuan Province (2022NSFSC0774), the National Natural Science Foundation of China (no. 82273030 and 82472869), and the 2021 Xinrui Tumor Supportive Treatment Research Public Welfare Project (no. 311221042). We thank Professor Yuquan Wei for his assistance in this study. We would like to thank Xiaojiao Wang (Core Facilities of West China Hospital, Sichuan University, Chengdu, China), who assisted with the flow cytometry measurements. We also greatly appreciate Li Li (Institute of Clinical Pathology, West China Hospital, Sichuan University, Chengdu, Sichuan, China) for her help with the muti-color IHC staining experiment. Meanwhile, we also extend our gratitude to Sisi Wu, Xuemei Chen, Yanjing Zhang, and Yinchan Wang (Core Facilities of West China Hospital, Sichuan University, Chengdu, China) for their assistance in the construction of recombinant vectors. Furthermore, we would also like to appreciate Xiaoting Chen (Animal Experiment Center of West China Hospital, Sichuan University, Chengdu, China) for her help with the mice experiments. We thank Junshi Biosciences for providing PD-1 inhibitors. We also thank Shanghai Sinotech Genomics Co., Ltd. for providing single-cell sequencing services and Shanghai Personal Biotechnology Co., Ltd. for offering PD-L1 lactylation-modified shotgun identification, targeted amino acid metabolomics, targeted organic acid metabolomics, and TCR sequencing services. Finally, we also thank BioRender.com, which helped us create schema charts.

AUTHOR CONTRIBUTIONS

X.M., H.S., Z. Lei, H.T., and Z.J. conceptualized and designed the study. X.M., H.S., and Z. Lei supervised the project. K.T., X. Li, H.Y., Q.K., Z. Long, J.Y., Q.L., X. Liang, Y. Wan, N.L., and X. Yang collected clinical samples and patient data. H.T., L.S., X. Yin, X. Li, G.L., and Y. Zhao executed the experimental protocols. Z.J. performed bioinformatics analysis of single-cell sequencing data. H.T., Z.J., K.T., X. Yin, and L.S. wrote the manuscript. H.T., Y. Wei, L.S., and Y. Zhao drew some figures. Z. Long and J.Y. executed the nutrition assessment of the enrolled patients. All co-authors, especially R.L. and X. Yin, helped review and edit the manuscript. All authors have agreed to be personally accountable for their own contributions and to ensure that questions related to the accuracy or integrity of any part of the work are answered.

DECLARATION OF INTERESTS

The authors C.H. and Z. Lei are shareholders and board members of Recovery Plus Clinic Co., which develops medical digital devices and nutritional powder for clinicians. Z. Long and J.Y. are also members of this company. Additionally, Recovery Plus Clinic Co. funded the targeted amino acid metabolism and some other sequencing services for this project. Their involvement could potentially bias the results, but independent analyses and unaffiliated researchers were included for study design and data analysis to minimize this possible risk.

DECLARATION OF GENERATIVE AI AND AI-ASSISTED TECHNOLOGIES IN THE WRITING PROCESS

During the preparation of this work the authors used ChatGPT-4 in order to translate and polish. After using this tool/service, the authors reviewed and edited the content as needed and take full responsibility for the content of the published article.

STAR★METHODS

Detailed methods are provided in the online version of this paper and include the following:

SUPPLEMENTAL INFORMATION

Supplemental information can be found online at https://doi.org/10.1016/j.cmet.2024.10.019.

Received: December 12, 2023
Revised: July 29, 2024
Accepted: October 21, 2024
Published: November 21, 2024

REFERENCES

1. Burnett-Hartman, A.N., Lee, J.K., Demb, J., and Gupta, S. (2021). An update on the epidemiology, molecular characterization, diagnosis, and screening strategies for early-onset colorectal cancer. Gastroenterology *160*, 1041–1049. https://doi.org/10.1053/j.gastro.2020.12.068.

2. Keum, N., and Giovannucci, E. (2019). Global burden of colorectal cancer: emerging trends, risk factors and prevention strategies. Nat. Rev. Gastroenterol. Hepatol. *16*, 713–732. https://doi.org/10.1038/s41575-019-0189-8.

3. Morse, M.A., Hochster, H., and Benson, A. (2020). Perspectives on treatment of metastatic colorectal cancer with immune checkpoint inhibitor therapy. Oncologist *25*, 33–45. https://doi.org/10.1634/theoncologist.2019-0176.

4. Ganesh, K., Stadler, Z.K., Cercek, A., Mendelsohn, R.B., Shia, J., Segal, N.H., and Diaz, L.A., Jr. (2019). Immunotherapy in colorectal cancer: rationale, challenges and potential. Nat. Rev. Gastroenterol. Hepatol. *16*, 361–375. https://doi.org/10.1038/s41575-019-0126-x.

5. Lizardo, D.Y., Kuang, C., Hao, S., Yu, J., Huang, Y., and Zhang, L. (2020). Immunotherapy efficacy on mismatch repair-deficient colorectal cancer: from bench to bedside. Biochim. Biophys. Acta Rev. Cancer *1874*, 188447. https://doi.org/10.1016/j.bbcan.2020.188447.

6. Kather, J.N., Halama, N., and Jaeger, D. (2018). Genomics and emerging biomarkers for immunotherapy of colorectal cancer. Semin. Cancer Biol. *52*, 189–197. https://doi.org/10.1016/j.semcancer.2018.02.010.

7. Kishore, C., and Bhadra, P. (2021). Current advancements and future perspectives of immunotherapy in colorectal cancer research. Eur. J. Pharmacol. *893*, 173819. https://doi.org/10.1016/j.ejphar.2020.173819.

8. Asaka, S., Arai, Y., Nishimura, Y., Yamaguchi, K., Ishikubo, T., Yatsuoka, T., Tanaka, Y., and Akagi, K. (2009). Microsatellite instability-low colorectal cancer acquires a KRAS mutation during the progression from Dukes' A to Dukes' B. Carcinogenesis *30*, 494–499. https://doi.org/10.1093/carcin/bgp017.

9. Akin Telli, T., Bregni, G., Vanhooren, M., Saude Conde, R., Hendlisz, A., and Sclafani, F. (2022). Regorafenib in combination with immune checkpoint inhibitors for mismatch repair proficient (pMMR)/microsatellite stable (MSS) colorectal cancer. Cancer Treat. Rev. *110*, 102460. https://doi.org/10.1016/j.ctrv.2022.102460.

10. Xia, J., Xie, Z., Niu, G., Lu, Z., Wang, Z., Xing, Y., Ren, J., Hu, Z., Hong, R., Cao, Z., et al. (2023). Single-cell landscape and clinical outcomes of infiltrating B cells in colorectal cancer. Immunology *168*, 135–151. https://doi.org/10.1111/imm.13568.

11. Li, J., Wu, C., Hu, H., Qin, G., Wu, X., Bai, F., Zhang, J., Cai, Y., Huang, Y., Wang, C., et al. (2023). Remodeling of the immune and stromal cell compartment by PD-1 blockade in mismatch repair-deficient colorectal cancer. Cancer Cell *41*, 1152–1169.e7. https://doi.org/10.1016/j.ccell.2023.04.011.

12. Sanz-Pamplona, R., Melas, M., Maoz, A., Schmit, S.L., Rennert, H., Lejbkowicz, F., Greenson, J.K., Sanjuan, X., Lopez-Zambrano, M., Alonso, M.H., et al. (2020). Lymphocytic infiltration in stage II microsatellite stable colorectal tumors: A retrospective prognosis biomarker analysis. PLoS Med. *17*, e1003292. https://doi.org/10.1371/journal.pmed.1003292.

13. Giannakis, M., Mu, X.J., Shukla, S.A., Qian, Z.R., Cohen, O., Nishihara, R., Bahl, S., Cao, Y., Amin-Mansour, A., Yamauchi, M., et al. (2016). Genomic correlates of immune-cell infiltrates in colorectal carcinoma. Cell Rep. *15*, 857–865. https://doi.org/10.1016/j.celrep.2016.03.075.

14. Lin, A., Zhang, J., and Luo, P. (2020). Crosstalk between the MSI status and tumor microenvironment in colorectal cancer. Front. Immunol. *11*, 2039. https://doi.org/10.3389/fimmu.2020.02039.

15. Locasale, J.W. (2013). Serine, glycine and one-carbon units: cancer metabolism in full circle. Nat. Rev. Cancer *13*, 572–583. https://doi.org/10.1038/nrc3557.

16. Amelio, I., Cutruzzolá, F., Antonov, A., Agostini, M., and Melino, G. (2014). Serine and glycine metabolism in cancer. Trends Biochem. Sci. *39*, 191–198. https://doi.org/10.1016/j.tibs.2014.02.004.

17. Wei, F., and Locasale, J.W. (2023). Methionine restriction and antitumor immunity. Trends Cancer *9*, 705–706. https://doi.org/10.1016/j.trecan.2023.07.008.

18. Wang, Z., Yip, L.Y., Lee, J.H.J., Wu, Z., Chew, H.Y., Chong, P.K.W., Teo, C.C., Ang, H.Y.K., Peh, K.L.E., Yuan, J., et al. (2019). Methionine is a metabolic dependency of tumor-initiating cells. Nat. Med. *25*, 825–837. https://doi.org/10.1038/s41591-019-0423-5.

19. Ngo, B., Kim, E., Osorio-Vasquez, V., Doll, S., Bustraan, S., Liang, R.J., Luengo, A., Davidson, S.M., Ali, A., Ferraro, G.B., et al. (2020). Limited environmental serine and glycine confer brain metastasis sensitivity to PHGDH inhibition. Cancer Discov. *10*, 1352–1373. https://doi.org/10.1158/2159-8290.CD-19-1228.

20. Hoffman, R.M., and Erbe, R.W. (1976). High in vivo rates of methionine biosynthesis in transformed human and malignant rat cells auxotrophic for methionine. Proc. Natl. Acad. Sci. USA *73*, 1523–1527. https://doi.org/10.1073/pnas.73.5.1523.

21. Montrose, D.C., Saha, S., Foronda, M., McNally, E.M., Chen, J., Zhou, X.K., Ha, T., Krumsiek, J., Buyukozkan, M., Verma, A., et al. (2021). Exogenous and endogenous sources of serine contribute to colon cancer metabolism, growth, and resistance to 5-fluorouracil. Cancer Res. *81*, 2275–2288. https://doi.org/10.1158/0008-5472.CAN-20-1541.

22. Gao, X., Sanderson, S.M., Dai, Z., Reid, M.A., Cooper, D.E., Lu, M., Richie, J.P., Jr., Ciccarella, A., Calcagnotto, A., Mikhael, P.G., et al. (2019). Dietary methionine influences therapy in mouse cancer models and alters human metabolism. Nature *572*, 397–401. https://doi.org/10.1038/s41586-019-1437-3.

23. Hosios, A.M., Hecht, V.C., Danai, L.V., Johnson, M.O., Rathmell, J.C., Steinhauser, M.L., Manalis, S.R., and Vander Heiden, M.G. (2016). Amino acids Rather than glucose account for the majority of cell mass in proliferating mammalian cells. Dev. Cell *36*, 540–549. https://doi.org/10.1016/j.devcel.2016.02.012.

24. Sonveaux, P., Copetti, T., De Saedeleer, C.J., Végran, F., Verrax, J., Kennedy, K.M., Moon, E.J., Dhup, S., Danhier, P., Frérart, F., et al. (2012). Targeting the lactate transporter MCT1 in endothelial cells inhibits lactate-induced HIF-1 activation and tumor angiogenesis. PLOS One *7*, e33418. https://doi.org/10.1371/journal.pone.0033418.

25. Lee, D.C., Sohn, H.A., Park, Z.Y., Oh, S., Kang, Y.K., Lee, K.M., Kang, M., Jang, Y.J., Yang, S.J., Hong, Y.K., et al. (2015). A lactate-induced response to hypoxia. Cell *161*, 595–609. https://doi.org/10.1016/j.cell.2015.03.011.

26. Végran, F., Boidot, R., Michiels, C., Sonveaux, P., and Feron, O. (2011). Lactate influx through the endothelial cell monocarboxylate transporter MCT1 supports an NF-κB/IL-8 pathway that drives tumor angiogenesis. Cancer Res. *71*, 2550–2560. https://doi.org/10.1158/0008-5472.CAN-10-2828.

27. Lunt, S.Y., and Vander Heiden, M.G. (2011). Aerobic glycolysis: meeting the metabolic requirements of cell proliferation. Annu. Rev. Cell Dev. Biol. *27*, 441–464. https://doi.org/10.1146/annurev-cellbio-092910-154237.

28. Colegio, O.R., Chu, N.Q., Szabo, A.L., Chu, T., Rhebergen, A.M., Jairam, V., Cyrus, N., Brokowski, C.E., Eisenbarth, S.C., Phillips, G.M., et al. (2014). Functional polarization of tumour-associated macrophages by tumour-derived lactic acid. Nature *513*, 559–563. https://doi.org/10.1038/nature13490.

29. Brand, A., Singer, K., Koehl, G.E., Kolitzus, M., Schoenhammer, G., Thiel, A., Matos, C., Bruss, C., Klobuch, S., Peter, K., et al. (2016). LDHA-associated lactic acid production blunts tumor immunosurveillance by T and NK cells. Cell Metab. *24*, 657–671. https://doi.org/10.1016/j.cmet.2016.08.011.

30. Haas, R., Smith, J., Rocher-Ros, V., Nadkarni, S., Montero-Melendez, T., D'Acquisto, F., Bland, E.J., Bombardieri, M., Pitzalis, C., Perretti, M., et al. (2015). Lactate regulates metabolic and pro-inflammatory circuits in control of T cell migration and effector functions. PLoS Biol. *13*, e1002202. https://doi.org/10.1371/journal.pbio.1002202.

31. Kumagai, S., Koyama, S., Itahashi, K., Tanegashima, T., Lin, Y.T., Togashi, Y., Kamada, T., Irie, T., Okumura, G., Kono, H., et al. (2022). Lactic acid promotes PD-1 expression in regulatory T cells in highly glycolytic tumor microenvironments. Cancer Cell *40*, 201–218.e9. https://doi.org/10.1016/j.ccell.2022.01.001.

32. Li, Z., and Yin, P. (2023). Tumor microenvironment diversity and plasticity in cancer multidrug resistance. Biochim. Biophys. Acta Rev. Cancer *1878*, 188997. https://doi.org/10.1016/j.bbcan.2023.188997.

33. Erin, N., Grahovac, J., Brozovic, A., and Efferth, T. (2020). Tumor microenvironment and epithelial mesenchymal transition as targets to overcome tumor multidrug resistance. Drug Resist. Updat. *53*, 100715. https://doi.org/10.1016/j.drup.2020.100715.

34. Tan, C.L., Lindner, K., Boschert, T., Meng, Z., Rodriguez Ehrenfried, A., De Roia, A., Haltenhof, G., Faenza, A., Imperatore, F., Bunse, L., et al. (2024). Prediction of tumor-reactive T cell receptors from scRNA-seq data for personalized T cell therapy. Nat. Biotechnol. https://doi.org/10.1038/s41587-024-02161-y.

35. Li, Y., Ji, L., Zhang, Y., Zhang, J., Reuben, A., Zeng, H., Huang, Q., Wei, Q., Tan, S., Xia, X., et al. (2024). The combination of tumor mutational burden and T-cell receptor repertoire predicts the response to immunotherapy in patients with advanced non-small cell lung cancer. Med. *5*, e604. https://doi.org/10.1002/mco2.604.

36. Yang, Z., Yan, C., Ma, J., Peng, P., Ren, X., Cai, S., Shen, X., Wu, Y., Zhang, S., Wang, X., et al. (2023). Lactylome analysis suggests lactylation-dependent mechanisms of metabolic adaptation in hepatocellular carcinoma. Nat. Metab. *5*, 61–79. https://doi.org/10.1038/s42255-022-00710-w.

37. Kotsiliti, E. (2023). Lactylation and HCC progression. Nat. Rev. Gastroenterol. Hepatol. *20*, 131. https://doi.org/10.1038/s41575-023-00746-7.

38. Fan, M., Yang, K., Wang, X., Chen, L., Gill, P.S., Ha, T., Liu, L., Lewis, N.H., Williams, D.L., and Li, C. (2023). Lactate promotes endothelial-to-mesenchymal transition via Snail1 lactylation after myocardial infarction. Sci. Adv. *9*, eadc9465. https://doi.org/10.1126/sciadv.adc9465.

39. Yi, M., Zhang, J., Li, A., Niu, M., Yan, Y., Jiao, Y., Luo, S., Zhou, P., and Wu, K. (2021). The construction, expression, and enhanced anti-tumor activity of YM101: a bispecific antibody simultaneously targeting TGF-β and PD-L1. J. Hematol. Oncol. *14*, 27. https://doi.org/10.1186/s13045-021-01045-x.

40. Xiong, J., He, J., Zhu, J., Pan, J., Liao, W., Ye, H., Wang, H., Song, Y., Du, Y., Cui, B., et al. (2022). Lactylation-driven METTL3-mediated RNA m(6)A modification promotes immunosuppression of tumor-infiltrating myeloid cells. Mol. Cell *82*, 1660–1677.e1610. https://doi.org/10.1016/j.molcel.2022.02.033.

41. Miao, Y., Du, Q., Zhang, H.G., Yuan, Y., Zuo, Y., and Zheng, H. (2023). Cycloheximide (CHX) chase assay to examine protein half-life. Bio Protoc. *13*, e4690. https://doi.org/10.21769/BioProtoc.4690.

42. Chalabi, M., Fanchi, L.F., Dijkstra, K.K., Van den Berg, J.G., Aalbers, A.G., Sikorska, K., Lopez-Yurda, M., Grootscholten, C., Beets, G.L., Snaebjornsson, P., et al. (2020). Neoadjuvant immunotherapy leads to pathological responses in MMR-proficient and MMR-deficient early-stage colon cancers. Nat. Med. *26*, 566–576. https://doi.org/10.1038/s41591-020-0805-8.

43. Bortolomeazzi, M., Keddar, M.R., Montorsi, L., Acha-Sagredo, A., Benedetti, L., Temelkovski, D., Choi, S., Petrov, N., Todd, K., Wai, P., et al. (2021). Immunogenomics of colorectal cancer response to checkpoint blockade: analysis of the KEYNOTE 177 trial and validation cohorts. Gastroenterology *161*, 1179–1193. https://doi.org/10.1053/j.gastro.2021.06.064.

44. Maddocks, O.D.K., Berkers, C.R., Mason, S.M., Zheng, L., Blyth, K., Gottlieb, E., and Vousden, K.H. (2013). Serine starvation induces stress and p53-dependent metabolic remodelling in cancer cells. Nature *493*, 542–546. https://doi.org/10.1038/nature11743.

45. Muthusamy, T., Cordes, T., Handzlik, M.K., You, L., Lim, E.W., Gengatharan, J., Pinto, A.F.M., Badur, M.G., Kolar, M.J., Wallace, M., et al. (2020). Serine restriction alters sphingolipid diversity to constrain tumour growth. Nature *586*, 790–795. https://doi.org/10.1038/s41586-020-2609-x.

46. Maddocks, O.D.K., Athineos, D., Cheung, E.C., Lee, P., Zhang, T., van den Broek, N.J.F., Mackay, G.M., Labuschagne, C.F., Gay, D., Kruiswijk, F., et al. (2017). Modulating the therapeutic response of tumours to dietary serine and glycine starvation. Nature *544*, 372–376. https://doi.org/10.1038/nature22056.

47. Ma, E.H., Bantug, G., Griss, T., Condotta, S., Johnson, R.M., Samborska, B., Mainolfi, N., Suri, V., Guak, H., Balmer, M.L., et al. (2017). Serine is an essential metabolite for effector T cell expansion. Cell Metab. *25*, 345–357. https://doi.org/10.1016/j.cmet.2016.12.011.

48. Wang, W., and Zou, W. (2020). Amino acids and their transporters in T cell immunity and cancer therapy. Mol. Cell *80*, 384–395. https://doi.org/10.1016/j.molcel.2020.09.006.

49. Chen, G., Zheng, D., Zhou, Y., Du, S., and Zeng, Z. (2024). Olaparib enhances radiation-induced systemic anti-tumor effects via activating STING-chemokine signaling in hepatocellular carcinoma. Cancer Lett. *582*, 216507. https://doi.org/10.1016/j.canlet.2023.216507.

50. Lee, K.M., Lin, C.C., Servetto, A., Bae, J., Kandagatla, V., Ye, D., Kim, G., Sudhan, D.R., Mendiratta, S., González Ericsson, P.I., et al. (2022). Epigenetic repression of STING by MYC promotes immune evasion and resistance to immune checkpoint inhibitors in triple-negative breast cancer. Cancer Immunol. Res. *10*, 829–843. https://doi.org/10.1158/2326-6066.CIR-21-0826.

51. Grygorczuk, S., Czupryna, P., Dunaj, J., Moniuszko-Malinowska, A., Świerzbińska, R., and Pancewicz, S. (2021). The chemotactic cytokines in the cerebrospinal fluid of patients with neuroborreliosis. Cytokine *142*, 155490. https://doi.org/10.1016/j.cyto.2021.155490.

52. Lozano, A.X., Chaudhuri, A.A., Nene, A., Bacchiocchi, A., Earland, N., Vesely, M.D., Usmani, A., Turner, B.E., Steen, C.B., Luca, B.A., et al. (2022). T cell characteristics associated with toxicity to immune checkpoint blockade in patients with melanoma. Nat. Med. *28*, 353–362. https://doi.org/10.1038/s41591-021-01623-z.

53. Finnigan, J.P., Newman, J.H., Patskovsky, Y., Patskovska, L., Ishizuka, A.S., Lynn, G.M., Seder, R.A., Krogsgaard, M., and Bhardwaj, N. (2024). Structural basis for self-discrimination by neoantigen-specific TCRs. Nat. Commun. *15*, 2140. https://doi.org/10.1038/s41467-024-46367-9.

54. Cheung, P.F., Yang, J., Fang, R., Borgers, A., Krengel, K., Stoffel, A., Althoff, K., Yip, C.W., Siu, E.H.L., Ng, L.W.C., et al. (2022). Progranulin mediates immune evasion of pancreatic ductal adenocarcinoma through regulation of MHCI expression. Nat. Commun. *13*, 156. https://doi.org/10.1038/s41467-021-27088-9.

55. Lauss, M., Phung, B., Borch, T.H., Harbst, K., Kaminska, K., Ebbesson, A., Hedenfalk, I., Yuan, J., Nielsen, K., Ingvar, C., et al. (2024). Molecular patterns of resistance to immune checkpoint blockade in melanoma. Nat. Commun. *15*, 3075. https://doi.org/10.1038/s41467-024-47425-y.

56. Buck, M.D., O'Sullivan, D., and Pearce, E.L. (2015). T cell metabolism drives immunity. J. Exp. Med. *212*, 1345–1360. https://doi.org/10.1084/jem.20151159.

57. Wei, J., Raynor, J., Nguyen, T.L.M., and Chi, H. (2017). Nutrient and metabolic sensing in T cell responses. Front. Immunol. *8*, 247. https://doi.org/10.3389/fimmu.2017.00247.

58. Almeida, L., Lochner, M., Berod, L., and Sparwasser, T. (2016). Metabolic pathways in T cell activation and lineage differentiation. Semin. Immunol. *28*, 514–524. https://doi.org/10.1016/j.smim.2016.10.009.

59. Chapman, N.M., Boothby, M.R., and Chi, H. (2020). Metabolic coordination of T cell quiescence and activation. Nat. Rev. Immunol. *20*, 55–70. https://doi.org/10.1038/s41577-019-0203-y.

60. Chen, H., Yang, T., Zhu, L., and Zhao, Y. (2015). Cellular metabolism on T-cell development and function. Int. Rev. Immunol. *34*, 19–33. https://doi.org/10.3109/08830185.2014.902452.

61. Feng, Q., Liu, Z., Yu, X., Huang, T., Chen, J., Wang, J., Wilhelm, J., Li, S., Song, J., Li, W., et al. (2022). Lactate increases stemness of CD8 + T cells to augment anti-tumor immunity. Nat. Commun. *13*, 4981. https://doi.org/10.1038/s41467-022-32521-8.

62. Huang, X., Zhang, Q., Lou, Y., Wang, J., Zhao, X., Wang, L., Zhang, X., Li, S., Zhao, Y., Chen, Q., et al. (2019). USP22 deubiquitinates CD274 to suppress anticancer immunity. Cancer Immunol. Res. *7*, 1580–1590. https://doi.org/10.1158/2326-6066.CIR-18-0910.

63. Lefrancois, S. (2019). Tumour suppression by blocking palmitoylation. Nat. Biomed. Eng. *3*, 255–256. https://doi.org/10.1038/s41551-019-0383-6.

64. Yang, H., Zhang, X., Lao, M., Sun, K., He, L., Xu, J., Duan, Y., Chen, Y., Ying, H., Li, M., et al. (2023). Targeting ubiquitin-specific protease 8 sensitizes anti-programmed death-ligand 1 immunotherapy of pancreatic cancer. Cell Death Differ. *30*, 560–575. https://doi.org/10.1038/s41418-022-01102-z.

65. Shi, C., Wang, Y., Wu, M., Chen, Y., Liu, F., Shen, Z., Wang, Y., Xie, S., Shen, Y., Sang, L., et al. (2022). Promoting anti-tumor immunity by targeting TMUB1 to modulate PD-L1 polyubiquitination and glycosylation. Nat. Commun. *13*, 6951. https://doi.org/10.1038/s41467-022-34346-x.

66. Huang, C., Ren, S., Chen, Y., Liu, A., Wu, Q., Jiang, T., Lv, P., Song, D., Hu, F., Lan, J., et al. (2023). PD-L1 methylation restricts PD-L1/PD-1 interactions to control cancer immune surveillance. Sci. Adv. *9*, eade4186. https://doi.org/10.1126/sciadv.ade4186.

67. Liu, Z., Wang, T., She, Y., Wu, K., Gu, S., Li, L., Dong, C., Chen, C., and Zhou, Y. (2021). N(6)-methyladenosine-modified circIGF2BP3 inhibits CD8(+) T-cell responses to facilitate tumor immune evasion by promoting the deubiquitination of PD-L1 in non-small cell lung cancer. Mol. Cancer *20*, 105. https://doi.org/10.1186/s12943-021-01398-4.

68. Yao, H., Lan, J., Li, C., Shi, H., Brosseau, J.P., Wang, H., Lu, H., Fang, C., Zhang, Y., Liang, L., et al. (2019). Inhibiting PD-L1 palmitoylation enhances T-cell immune responses against tumours. Nat. Biomed. Eng. *3*, 306–317. https://doi.org/10.1038/s41551-019-0375-6.

69. Wang, Y.N., Lee, H.H., Hsu, J.L., Yu, D., and Hung, M.C. (2020). The impact of PD-L1 N-linked glycosylation on cancer therapy and clinical diagnosis. J. Biomed. Sci. *27*, 77. https://doi.org/10.1186/s12929-020-00670-x.

70. Ji, P., Wu, P., Wang, L., Wang, Y., Guo, X., Gao, R., Guo, Z., Zhou, H., Liu, Z., Liang, Y., et al. (2024). Lysosome-targeting bacterial outer membrane vesicles for tumor specific degradation of PD-L1. Small *20*, e2400770. https://doi.org/10.1002/smll.202400770.

71. Luo, J., Gao, Q., Tan, K., Zhang, S., Shi, W., Luo, L., Li, Z., Khedr, G.E., Chen, J., Xu, Y., et al. (2024). Lysosome targeting chimaeras for Glut1-facilitated targeted protein degradation. J. Am. Chem. Soc. *146*, 17728–17737. https://doi.org/10.1021/jacs.4c02463.

72. Xu, X., Xie, T., Zhou, M., Sun, Y., Wang, F., Tian, Y., Chen, Z., Xie, Y., Wu, R., Cen, X., et al. (2024). Hsc70 promotes anti-tumor immunity by targeting PD-L1 for lysosomal degradation. Nat. Commun. *15*, 4237. https://doi.org/10.1038/s41467-024-48597-3.

73. Ahn, G., Riley, N.M., Kamber, R.A., Wisnovsky, S., Moncayo von Hase, S., Bassik, M.C., Banik, S.M., and Bertozzi, C.R. (2023). Elucidating the cellular determinants of targeted membrane protein degradation by lysosome-targeting chimeras. Science *382*, eadf6249. https://doi.org/10.1126/science.adf6249.

74. Burr, M.L., Sparbier, C.E., Chan, Y.C., Williamson, J.C., Woods, K., Beavis, P.A., Lam, E.Y.N., Henderson, M.A., Bell, C.C., Stolzenburg, S., et al. (2017). CMTM6 maintains the expression of PD-L1 and regulates anti-tumour immunity. Nature *549*, 101–105. https://doi.org/10.1038/nature23643.

75. Wang, Q., Wang, J., Yu, D., Zhang, Q., Hu, H., Xu, M., Zhang, H., Tian, S., Zheng, G., Lu, D., et al. (2024). Benzosceptrin C induces lysosomal degradation of PD-L1 and promotes antitumor immunity by targeting DHHC3. Cell Rep. Med. *5*, 101357. https://doi.org/10.1016/j.xcrm.2023.101357.

76. Zyss, D., Montcourrier, P., Vidal, B., Anguille, C., Mérezègue, F., Sahuquet, A., Mangeat, P.H., and Coopman, P.J. (2005). The Syk tyrosine kinase localizes to the centrosomes and negatively affects mitotic progression. Cancer Res. *65*, 10872–10880. https://doi.org/10.1158/0008-5472.CAN-05-1270.

77. Zu, Y., Liu, L., Lee, M.Y.K., Xu, C., Liang, Y., Man, R.Y., Vanhoutte, P.M., and Wang, Y. (2010). SIRT1 promotes proliferation and prevents senescence through targeting LKB1 in primary porcine aortic endothelial cells. Circ. Res. *106*, 1384–1393. https://doi.org/10.1161/CIRCRESAHA.109.215483.

78. Zientara-Rytter, K., and Subramani, S. (2016). Role of actin in shaping autophagosomes. Autophagy *12*, 2512–2515. https://doi.org/10.1080/15548627.2016.1236877.

79. Zhu, Y., Zhao, L., Liu, L., Gao, P., Tian, W., Wang, X., Jin, H., Xu, H., and Chen, Q. (2010). Beclin 1 cleavage by caspase-3 inactivates autophagy and promotes apoptosis. Protein Cell *1*, 468–477. https://doi.org/10.1007/s13238-010-0048-4.

80. Aguilera, M.O., Berón, W., and Colombo, M.I. (2012). The actin cytoskeleton participates in the early events of autophagosome formation upon starvation induced autophagy. Autophagy *8*, 1590–1603. https://doi.org/10.4161/auto.21459.

81. Huang, Z.W., Zhang, X.N., Zhang, L., Liu, L.L., Zhang, J.W., Sun, Y.X., Xu, J.Q., Liu, Q., and Long, Z.J. (2023). STAT5 promotes PD-L1 expression by facilitating histone lactylation to drive immunosuppression in acute myeloid leukemia. Signal Transduct. Target. Ther. *8*, 391. https://doi.org/10.1038/s41392-023-01605-2.

82. Zhang, D., Tang, Z., Huang, H., Zhou, G., Cui, C., Weng, Y., Liu, W., Kim, S., Lee, S., Perez-Neut, M., et al. (2019). Metabolic regulation of gene expression by histone lactylation. Nature *574*, 575–580. https://doi.org/10.1038/s41586-019-1678-1.

83. Yu, J., Chai, P., Xie, M., Ge, S., Ruan, J., Fan, X., and Jia, R. (2021). Histone lactylation drives oncogenesis by facilitating m(6)A reader protein YTHDF2 expression in ocular melanoma. Genome Biol. *22*, 85. https://doi.org/10.1186/s13059-021-02308-z.

84. Zhao, Y., Zhang, M., Huang, X., Liu, J., Sun, Y., Zhang, F., Zhang, N., and Lei, L. (2024). Lactate modulates zygotic genome activation through H3K18 lactylation rather than H3K27 acetylation. Cell. Mol. Life Sci. *81*, 298. https://doi.org/10.1007/s00018-024-05349-2.

85. Venegas-Borsellino, C., and Kwon, M. (2019). Impact of soluble fiber in the microbiome and outcomes in critically ill patients. Curr. Nutr. Rep. *8*, 347–355. https://doi.org/10.1007/s13668-019-00299-9.

86. Camilleri, M. (2021). Human intestinal barrier: effects of stressors, diet, prebiotics, and probiotics. Clin. Transl. Gastroenterol. *12*, e00308. https://doi.org/10.14309/ctg.0000000000000308.

87. Zhao, R., Wang, Y., Huang, Y., Cui, Y., Xia, L., Rao, Z., Zhou, Y., and Wu, X. (2017). Effects of fiber and probiotics on diarrhea associated with enteral nutrition in gastric cancer patients: A prospective randomized and controlled trial. Med. (Baltim.) *96*, e8418. https://doi.org/10.1097/MD.0000000000008418.

88. Sun, H., Li, X., Chen, W., Jia, F., Su, J., Zhang, B., Wu, X., and Wu, P. (2021). Effect of probiotics and dietary fiber combined with pinaverium bromide on intestinal flora in patients with irritable bowel syndrome. Am. J. Transl. Res. *13*, 14039–14045.

STAR★METHODS

KEY RESOURCES TABLE

REAGENT OR RESOURCES	SOURCE	IDENTIFIER
Antibodies		
Recombinant Anti-HMGB1 antibody [EPR3507]	Abcam	Cat# ab79823; RRID: AB_1603373
Recombinant Anti-Calreticulin antibody [EPR3924]	Abcam	Cat# ab92516; RRID: AB_10562796
Ki-67 (D3B5) Rabbit mAb	CST	Cat#12202S; RRID: AB_2620142
Granzyme B (D6E9W) Rabbit mAb	CST	Cat#46890S; RRID: AB_2799313
Anti-CD3 antibody [CD3-12]	Abcam	Cat# ab11089; RRID: AB_2889189
Recombinant Anti-CD4 antibody [EPR19514]	Abcam	Cat# ab183685; RRID: AB_2686917
Recombinant Anti-CD8 alpha antibody [EPR21769]	Abcam	Cat# ab217344; RRID: AB_2890649
HRP-conjugated Affinipure Goat Anti-Rat IgG(H+L)	Proteintech	Cat# SA00001-15; RRID: AB_2864369
CD68 Rabbit anti-Human, Mouse, Polyclonal	Proteintech	Cat# 25747-1-AP -15; RRID: AB_2721140
Rabbit IgG control Polyclonal antibody	Proteintech	Cat#30000-0-AP; RRID: AB_2819035
GAPDH polyclonal antibody	Bioworld	Cat#AP0063; RRID: AB_2651132
PD-L1/CD274 (C-terminal) Polyclonal antibody	Proteintech	Cat# 28076-1-AP; RRID: AB_2881052
PD-L1/CD274 Monoclonal antibody	Proteintech	Cat#66248-1; RRID: AB_2756526
Goat anti-Rabbit IgG(H+L)-HRP	Bioworld	Cat# BS13278; RRID: AB_2773728
Goat anti-mouse IgG(H+L)-HRP	Bioworld	Cat# BS12478; RRID: AB_2773727
Fixable Viability Dye eFluor™ 455UV	Invitrogen	Cat#65-0868-18; RRID: AB_2943687
CD45 Monoclonal Antibody (30-F11), Alexa Fluor™ 488	Invitrogen	Cat#53-0451-82; RRID: AB_2848416
CD45 Monoclonal Antibody (30-F11), Alexa Fluor™ 700	Invitrogen	Cat# 56-0451-82; RRID: AB_891454
CD3e Monoclonal Antibody (145-2C11), APC-eFluor™ 780	Invitrogen	Cat#47-0031-82; RRID: AB_11149861
CD8a Monoclonal Antibody (53-6.7), APC	Invitrogen	Cat#17-0081-82; RRID: AB_469335
CD274 (PD-L1, B7-H1) Monoclonal Antibody (MIH5), Super Bright™ 436	Invitrogen	Cat#62-5982-82; RRID: AB_2688095
CD326 (EpCAM) Monoclonal Antibody (G8.8), Super Bright™ 600	Invitrogen	Cat#63-5791-82; RRID: AB_2688099
Granzyme B Monoclonal Antibody (NGZB), PE-Cyanine7	Invitrogen	Cat#25-8898-82; RRID: AB_10853339
Ki-67 Monoclonal Antibody (SolA15), PerCP-eFluor™ 710	Invitrogen	Cat#46-5698-82; RRID: AB_11040981
IFN gamma Monoclonal Antibody (XMG1.2), PE	Invitrogen	Cat#12-7311-82; RRID: AB_466193
MHC Class II (I-A/I-E) Monoclonal Antibody (M5/114.15.2), PerCP-eFluor™ 710	Invitrogen	Cat#46-5321-82; RRID: AB_1834439
CD11b Monoclonal Antibody (M1/70), APC	Invitrogen	Cat#17-0112-81; RRID: AB_469342
Mouse Osteopontin/OPN PE-conjugated Antibody	R&D Systems	Cat# IC808P; RRID: AB_10643832
eBioscience™ Fixable Viability Dye eFluor™ 506	Invitrogen	Cat#65-0866-18; RRID: AB_2943689

(*Continued on next page*)

Continued

REAGENT OR RESOURCES	SOURCE	IDENTIFIER
CD45 Monoclonal Antibody (HI30), Brilliant Ultra Violet™ 496	Invitrogen	Cat# 364-0459-42; RRID: AB_2920964
CD3 Monoclonal Antibody (OKT3), Alexa Fluor™ 488	Invitrogen	Cat# 53-0037-42; RRID: AB_1907370
CD8a Monoclonal Antibody (RPA-T8), Super Bright™ 780	Invitrogen	Cat#78-0088-42; RRID: AB_2724102
IFN gamma Monoclonal Antibody (4S.B3), APC-eFluor™ 780	Invitrogen	Cat# 47-7319-42; RRID: AB_10853011
PE/Cyanine7 anti-human/mouse Granzyme B Recombinant Antibody	Biolegend	Cat# 372214; RRID: AB_2728381
Ki-67 Monoclonal Antibody (SolA15), APC	Invitrogen	Cat# 17-5698-82; RRID: AB_2688057
InVivoMab anti-mouse CD8β	BioXcell	Cat#BE0223; RRID:AB_2687706
Hexokinase 1 Polyclonal antibody	Proteintech	Cat# 19662-1-AP; RRID: AB_10859778
LDHA Monoclonal antibody	Proteintech	Cat# 66287-1-Ig; RRID: AB_2881670
PKM2 (D78A4) XP® Rabbit mAb #4053	CST	Cat# 4053S; RRID: AB_331163
PD-L1 (E1L3N®) XP® Rabbit mAb #13684	CST	Cat# 13684S; RRID: AB_2637077
HIF-1α (D1S7W) XP® Rabbit mAb #36169	CST	Cat# 36169S; RRID: AB_2798847
Chemicals, peptides, and recombinant proteins		
RPMI-1640 medium	GIBCO	Cat#C11875500BT
Fetal Bovine Serum	Sorfa	Cat# SX1500
DMEM medium	GIBCO	Cat#C11995500BT
Trypsin	GIBCO	Cat#25200072
Penicillin / Streptomycin / Amphotericin B, sterile solution	VICMED	Cat# VC2036
Collagenase, type 4	GIBCO	Cat#17104019
DNase I	Roche	Cat#63792800
Hyaluronidase from bovine testes	Sigma	Cat#H4272
Mouse Lymphocyte Separation Medium	Dakewe biotech	Cat#7211011
Red Blood Cell Lysis Buffer	Solarbio	Cat#R1010
Protein Phosphatase Inhibitor	Solarbio	Cat#P1260
DAPI Nuclear dye	FCMACS	Cat#FMS-FZ011-0100
DAB	CST	Cat#11725S
RIPA buffer	Beyotime	Cat#P0013B
PMSF	Beyotime	Cat#ST506
PageRuler Prestained Protein Ladder	Thermo Scientific	Cat#26616
BSA	Solarbio	Cat#A8020
Trizol	TIANGEN	Cat#DP424
Iron (III) nitrate nonahydrate	MACKLIN	Cat#I809398
Potassium chloride	Sangon Biotech	Cat#A501159
Magnesium sulfate	SCR	Cat#20025117
Sodium chloride	Sangon Biotech	Cat#A501218
Sodium phosphate, monobasic, anhydrous	Sangon Biotech	Cat#A501726
L-Arginine, free base	Sangon Biotech	Cat#A600205
L-Cystine	MACKLIN	Cat#C6205
L-Glutamine	MACKLIN	Cat#L810391
L-Histidine	Sangon Biotech	Cat#A604351
L-Isoleucine	SCR	Cat#62016031
L-Leucine	SCR	Cat#62015932
L-Lysine monohydrochloride	SCR	Cat#62017132
L-Threonine	SCR	Cat#62021634

(*Continued on next page*)

Continued

REAGENT OR RESOURCES	SOURCE	IDENTIFIER
L-Tryptophan	Sangon Biotech	Cat#A601911
L-Tyrosine	SCR	Cat#62023534
L-Valine	MACKLIN	Cat#V6271
Calcium D-pantothenatealanine hemicalcium salt	SCR	Cat#67000434
Folic acid	SCR	Cat#67000834
myo-Inositol	SCR	Cat#63007734
Nicotinamide	SCR	Cat#67000936
Riboflavin	MACKLIN	Cat#R817215
Thiamine hydrochloride	MACKLIN	Cat#T818865
Pyridoxine hydrochloride	MACKLIN	Cat#V820446
D-Glucose	Sangon Biotech	Cat#A501991
Sodium pyruvate	SCR	Cat#30169134
Phenol red	SCR	Cat#71032460
L-Methionine	SCR	Cat#62017434
L-Phenylalanine	SCR	Cat#62019234
Choline chloride	MACKLIN	Cat#C805028
NaHCO3	Sangon Biotech	Cat#A100865
L-Serine	Sigma	Cat#S4311
Glycine	SCR	Cat#62011516
Triton X-100	Biosharp	Cat#BS084
EDTA antigen repair solution pH9.0	ZSGB-BIO	Cat#ZLI-9069
Normal Goat Serum For Blocking	ZSGB-BIO	Cat#ZLI-9056
MTT	Beyotime	Cat#ST316
Diet with 1% Serine	Moldiets	M22071401
Diet without Serine and Glycine	Moldiets	M22070403
Critical commercial assays		
One Step TUNEL Apoptosis Assay Kit	Beyotime	Cat#C1086
EdU Flow Cytometry Assay Kits (Cy5)	APExbio	Cat#K1078
PrimeScript™ RT reagent Kit (Perfect Real Time)	Takara	Cat#RR036A
BCA Protein Assay Kit	Solarbio	Cat# PC0020
ImunoSepTM Mouse CD8+ Cell Positive Selection Kit	Precision BioMedicals	Cat#722805
Experimental models: Cell lines		
CT26	ATCC	CRL-2638
MC38	Abiowell Biotechnology CO., LTD (Changsha, China)	AW-CCM074
293T	National Collection of Authenticated Cell Cultures (Shanghai, China)	SCSP-502
Experimental models: Organisms/strains		
Balb/c mice	BEIJING HFK BIOSCIENCE CO.LTD	11002A
Balb/c nude mice	Beijing HFK Bioscience	13001A
Rag1 KO mice	Jiangsu Jicui Yakang Biotechnology	T004753
Biological samples		
Blood samples from patients	West China Hospital, Sichuan University	N/A
Blood samples from patients	Sichuan Provincial People's Hospital	N/A
Blood samples from patients	Xinjin District Hospital of Traditional Chinese Medicine	N/A

(*Continued on next page*)

Continued

REAGENT OR RESOURCES	SOURCE	IDENTIFIER
Oligonucleotides		
GAPDH forward: 5'-AGGTCGGTGTG AACGGATTTG-3'	This paper	N/A
GAPDH reverse: 5'- TGTAGACCAT GTAGTTGAGGTCA-3'	This paper	N/A
CD69 forward: 5'-TTACTTCTTCTCCA CCACAACCAAG -3'	This paper	N/A
CD69 reverse: 5'-AGCCCAATCCAAT GTTCCAGTTC -3'	This paper	N/A
CD28 forward: 5'-AGGCTGCTGTTCT TGGCTCTC -3'	This paper	N/A
CD28 reverse: 5'-AGGCTGACCTCGTT GCTATCTAC -3'	This paper	N/A
CXCL11 forward: 5'-ATTATGAGGCGAG CTTGCTTGG-3'	This paper	N/A
CXCL11 reverse: 5'-ACGGCTGCGACAA AGTTGAAG-3'	This paper	N/A
CXCL10 forward: 5'-CATCCTGCTGGG TCTGAGTGG -3'	This paper	N/A
CXCL10 reverse: 5'-GGCTCGCAGGGAT GATTTCAAG -3'	This paper	N/A
CCL5 forward: 5'-TGCTGCTTTGCCTAC CTCTCC-3'	This paper	N/A
CCL5 reverse: 5'-CACACACTTGGCG GTTCCTTC-3'	This paper	N/A
Recombinant DNA		
SLC12A4_shRNA1	CAGGGTAACCACAGAGAGAAT	N/A
SLC12A4_shRNA2	GCGACGAGAACTACATGGAAT	N/A
SLC12A4_shRNA3	CGTGCCTGGAAGACCTTTATT	N/A
PD-L1_shRNA1	CCGAAATGATACACAATTCGA	N/A
PD-L1_shRNA2	GCCACTTCTGAGCATGAACTA	N/A
PD-L1_shRNA3	GCGTTGAAGATACAAGCTCAA	N/A
Deposited data		
sc-RNA Seq	–	GEO: GSE276916
sc-TCR Seq	–	GEO: GSE276920
Sorftware and algorithms		
Graphpad prim 8	–	http://www.Graphpad.com
Image J	–	http://imagej.net/sorftware/imagej/
Qupath	–	http://qupath.github.io
Cell Ranger-3.0.0	–	http://10xgenomics.com/
R-4.2.1	–	https://www.r-project.org/
Seurat-4.0.1	–	https://satijalab.org/seurat/
ggplot2-3.3.3	–	https://cran.r-project.org/web/packages/ggplot2/
scRepertoire-2.0.0	–	https://bioconductor.org/packages/release/bioc/html/scRepertoire.html

EXPERIMENTAL MODEL AND STUDY PARTICIPANT DETAILS

Animals

Female Balb/c and Balb/c nude mice, aged 6–8 weeks, were acquired from HFK Bioscience. Similarly, Rag1 KO mice of the same age range were purchased from Jicui Yakang Biotechnology. All mice were bred in a specific pathogen-free (SPF) facility with a 12-hour light/dark cycle and with free access to food and water. In all experiments, mice were anaesthetized by isoflurane. All animal

experiments were approved by the Ethics Review Committee of Animal Experimentation of Sichuan University. All animal-handling procedures were performed according to the Guide for the Care and Use of Laboratory Animals of the National Institutes of Health and the guidelines of the Animal Welfare Act.

Patient material and Ethics

This single-arm, phase I study followed all relevant ethical regulations. From March 2022 to September 2023, blood samples were collected from patients who were enrolled in the West China Hospital of Sichuan University, Sichuan Provincial People's Hospital, and Xinjin District Hospital of Traditional Chinese Medicine. Written informed consent was obtained from the patients. The clinical trial in this study was approved by the Ethics Committee on Biomedical Research of West China Hospital, Sichuan Provincial People's Hospital, et al., and we complied with all relevant ethical regulations. Besides, this single-arm study registered in Chinese Clinical Trial Register (ChiCTR2300067929).

Patient inclusion and exclusion criteria for enrollment

Inclusion criteria

- Patients aged 18-70, gender not limited.
- BMI $\geq$ 18.5.
- NRS-2002 scale score < 3.
- Diagnosed with solid tumors in stage IIIa and above.
- Capable of oral intake or through gastric tube, tolerant for enteral nutrition.
- Willing to participate in the study and provide written informed consent.

Exclusion criteria

- Participate in other intervention clinical trials (including drugs, nutritional supplements, medical devices, etc.) within the first 4 weeks of screening.
- Presence of severe diarrhea, intractable vomiting, severe malabsorption syndrome, paralysis, mechanical intestinal obstruction, or active gastrointestinal bleeding.
- Allergy to sample components.
- Other nutritional supplements that may affect the effectiveness of the experiment are being used.
- Pregnant, lactating female patients or women with fertility who test positive in the baseline pregnancy test.
- Presence of cognitive impairments or mental illnesses that were unable to comprehend the research content.
- The researcher believes that it is not suitable to participate in this study.

Exit and suspension criteria

Exit criteria

- The subject requests to withdraw.
- Termination of study.
- The researcher believes that the subject will face unacceptable risks if he continues to participate in the study.
- Other circumstances requiring withdrawal.

Suspension criteria

- Serious adverse events occurred during the experimental process, and it was determined by the researchers that it needs to be terminated;
- BMI < 18.5.
- NRS-2002 scale score $\geq$ 3.
- Other circumstances that require suspension.

METHOD DETAILS

Cell culture

CT26, MC38, and 293T cells were cultured in RPMI-1640 and DMEM, respectively, supplemented with 10% fetal bovine serum (FBS), 1% Penicillin (100 U/mL), Streptomycin (100 μg/mL) and Amphotericin B (25 μg/mL) at 37 °C with 5% CO2 and maintained at a confluence of 70–80%. For all serine and glycine deprivation experiments, CT26 cells were cultured in complete medium and serine/glycine-free (-SG) medium, as described in Table S5. All components were dissolved in ddH2O and filtered through a 0.22 μm filter before use. Serine and glycine were prepared as 100× stocks in water and sterile filtered.

Cell proliferation and apoptosis assays

CT26 cells were seeded in 96-well plates and allowed to adhere overnight. Then the culture medium was replaced by complete and -SG medium respectively. After 48h, 72h and 96h, the cells were incubated with 5 mg/mL MTT solution (Beyotime) at 37 °C for an

additional 4h. DMSO was added into each well and gently mixed for 10 min. The absorbance was measured at a wavelength of 570 nm using a microplate reader (Biotek, USA). For the EdU incorporation assay, 10 μM EdU was added into each well for another 2 h, and proliferation was then analyzed using EdU Flow Cytometry Assay Kits (Cy5) (APExBIO) according to the manufacturer's instructions. For apoptosis assays, a One Step TUNNEL Apoptosis Assay Kit (Beyotime, C1086) was used following the manufacturer's protocol. Samples were detected by the BD LSRFortessa flow cytometry, and the results were analyzed with FlowJo V10 software.

Colony Formation Assay

CT26 cells were seeded at 400 cells/well in a 6-well plate with complete medium and allowed to adhere overnight. Then the culture medium was replaced by complete and -SG medium respectively. Cells were incubated for 12 days, fixed with 10% formalin, and stained with 0.1% crystal violet (Biosharp, BL802A). The wells were photographed and the colonies were counted.

Transwell migration assay

Transwell chambers (8μm pore size; Corning, USA) without matrigel were used to determine the migration ability of CT26 cells. In brief, 1×10^5 cells were suspended in 100 μL 1640 containing no FBS and added to the upper chamber, while 600 μL 1640 containing 10% FBS was placed in the lower chamber. After 6h of incubation, the cells remaining in the upper chamber were removed using cotton swabs. Cells on the lower surface of the membrane were fixed in 4% paraformaldehyde (PFA) and stained with 0.1% crystal violet (Biosharp, BL802A). Cells in 5 microscopic fields were counted and photographed. All experiments were performed in triplicate.

Detection of cell-surface PD-L1

Small-molecular compounds added in cell medium were FX11 (Selleck Chemicals, #S8928), MG-132 (MACKLIN, #M832899), Chloroquine (MACKLIN, #C843545), 3-MA (MACKKLIN, #M833793), NH4Cl (MACKLIN, #A801304), Pepstatin A (MACKLIN, #P816471), BAY-8002 (Selleck Chemicals, #S8747), 2-HG (Selleck Chemicals, #S1325), and CHX (Selleck Chemicals, #S7418), Lactate sodium - FITC (Xi'an ruixi bio, #RS0230105) for indicated time points. Collect cells and detect the expression levels of PD-L1 by Western Blot.

Immunomagnetic bead selection of CD8+ T cells

To prepare a single-cell suspension, the spleen was mechanically dissociated in lymphocyte separation solution. The suspension was centrifuged at 800g with slow acceleration and deceleration to isolate the intermediate white mononuclear lymphocyte layer, which was then counted. For every 10^7 cells, 2 μL of sorting reagent A was added, thoroughly mixed, and incubated at 4°C for 15 minutes. Post-incubation, 1 mL of separation buffer was added per 10^7 cells; the mixture was centrifuged at 300g for 5 minutes, and the supernatant was discarded. The cells were resuspended in 100 μL of separation buffer, mixed with 20 μL of sorting reagent B, and incubated again at 4°C for 15 minutes. After repeating the centrifugation under the same conditions, the supernatant was removed. The cells were finally resuspended in 2.5 mL of separation buffer, placed in a magnetic field for 5 minutes to bind CD8+ T cells, and the supernatant was quickly discarded. The washing step was repeated twice, and the bound CD8+ T cells were collected from the sorting tube.

Cell transfections Preparation

Short hairpin RNAs (shRNAs) targeting the mouse PD-L1 and SLC12A4 genes were synthesized by Sangon Biotech (Shanghai, China) and subsequently subcloned into the lentivirus vectors PLKO and pRRLsin.cPPT.CMV.Blasticidin (CPPT), respectively. Recombinant lentiviruses were produced using a third-generation lentiviral packaging system in HEK293T cells. These cells were transfected using the calcium phosphate method. The culture medium was replaced with fresh medium containing 10 mM sodium butyrate and 20 mM HEPES 12 hours post-transfection. After an additional 8 hours, it was again replaced with fresh medium solely containing 20 mM HEPES. Following a 16-hour incubation, the lentivirus-containing supernatant was collected, filtered through a 0.45 μm PVDF filter membrane (Millipore) to eliminate cellular debris, aliquoted, and stored at -80°C.

Stable cell line construction

For the SLC12A4 and PD-L1 knockdown CT26 cells and CD8+ T cells, the cells are infected with lentivirus and selected by 10 μg/mL puromycin. To generate the PD-L1 K to E CT26 cells, the wild type PD-L1 of CT26 cells are knocked down by shRNA and selected by puromycin firstly, and then infected with PD-L1 K to E lentivirus overexpression vector and selected by 200μg/mL Blasticidin. CT26 cells infected with PD-L1 wild type lentivirus overexpression vector serves as control. The lentiviruses are harvested and transfected with CT26 tumor cells. After 24-h-transfection, the tumor cells are screened with puromycin (for PLKO vector, Selleck, #S7417) or blasticidin (for CPPT vector, Invivogen, #ant-bl-1) obtain highly transduced cells.

In vivo mouse models

Prior to tumor cell injection, 6–8-week-old age-matched mice were shaved at the flank or colon. Recipients were switched from normal chow to a control or serine/glycine-free diet one week before inoculation. A total of 5×10^5 CT26, MC38, SLC12A4 knockdown CT26, PD-L1 knockdown CT26, or PD-L1 K to E CT26 cells in 100 μL PBS were subcutaneously inoculated into the right flank of the mice. Additionally, 2×10^6 CT26/MC38 cells in 30 μL PBS were orthotopically inoculated into the colon. For PD-1 antibody treatment,

100 μg of PD-1 antibody (Junshi Biosciences) or 100 μL PBS as a control was injected intraperitoneally on days 7, 10, and 13 post-CT26 cell inoculation. For CD4, CD8, and CSF1R antibody depletion treatments, 100 μL of 2 mg/mL anti-CD4 (Selleck, #A2101), anti-CD8 (BioXcell, #BE0223), anti-CSF1R antibody (Selleck, #A2159), or 100 μL PBS as a control was injected intraperitoneally on days -7, -3, 1, 5, and 9 post-CT26 cell inoculation. For the reintroduction of different CD8+ T cells, 3×10^5 CT26 cells in 100 μL PBS were subcutaneously inoculated into the right flank of 6–8-week-old female Balb/c nude mice, followed by the reinfusion of 2×10^6 T cells into the mice tail.Tumors were measured with a caliper, and tumor volume was calculated by the following formula: $1/2\times\text{length}\times\text{width}^2$. Control and serine and glycine-free diets were obtained from Moldiets.

Preparation of single-cell suspensions

We collected subcutaneous tumors from mice treated with control diet and -SG diet respectively. Tumors were cut into small pieces (<1 mm in diameter) on ice and then digested in 1 mg/mL collagenase type IV (Gibco, 17104019), 50 μg/mL DNase I (Roche, 63792800), and 100 μg/mL hyaluronidase (Sigma, H4272) in 5 mL of RPMI 1640 medium containing 10% FBS for 30 min on a 37 °C shaker. Next, 10 mL RPMI 1640 medium containing 10% FBS was added to dilute the suspensions. Then, the cell suspensions were passed through 40 μm cell strainers, and the lower layer was collected after centrifuging at 500g for 3min. Subsequently, the cells were washed and resuspended in PBS.

Single-cell RNA-seq library preparation and sequencing

Single-cell RNA-seq libraries were generated by the Chromium Next GEM Single Cell 3' Reagent Kits v3.1 by following the Chromium Next GEM Single Cell 3' Reagent Kits v3.1(Dual Index) User Guide. DNA libraries were run using the NovaSeq 6000 system (Illumina, San Diego, CA) to achieve roughly 500 million paired-end reads per sample. Constructed libraries were validated and quantified with the High Sensitivity DNA chip and by qPCR and subsequently sequenced on an Illumina NextSeq 500 in high-output mode. A total of 20,662 and 14,774 cells were sequenced from Balb/c mice, respectively.

Single-cell VDJ sequencing and analysis

The single cell suspension was loaded onto a 10× Chromium A Chip and the scRNA-Seq libraries were constructed following the protocol of the 10× genomics Chromium Single Cell Immune Profiling Solution. After the RT reaction, droplets were broken and barcoded-cDNA was purified with DynaBeads, followed by PCR-amplification. Sequencing libraries of single-cell transcriptomes suitable for Illumina sequencing platform were constructed after partial cDNA fragments and splicing. The remaining cDNA was enriched for the immune receptor (TCR), and the enriched products were amplified by PCR to construct a sequencing library suitable for the Illumina sequencing platform. Finally, each library was sequenced on Illumina NovaSeq X plus with 150 bp paired-end reads. Average sequencing depth aimed for the mRNA library is 34,532 read pairs per cell and 157,632 read pairs per cell for the VDJ libraries. Diversity and clonality analysis of single cell TCR-seq data were done thanks to scRepertoire package.

Pre-processing of single-cell RNA-seq data

scRNA-seq data were aligned and quantified using the CellRanger toolkit v.3.1 against the mm10 reference genome. To exclude low-quality cells and cells that were extreme outliers in terms of library complexity, we calculated the distribution of genes detected per cell, UMIs, and the proportion of mitochondrial genes. Then, the qualities of cells and genes were assessed by 4 standards: (1) Cells with expressed genes over 6,000 or less than 400 were filtered. (2) Cells with a total UMI count over 30,000 or less than 600 were filtered. (3) Cells that have over 10% mitochondrial counts were filtered. (4) Genes expressed in fewer than 0.1% of cells within a sample were removed. Next, we employed a combination of three methods to identify potential doublets. For each sample, we used DoubleFinder, Scrublet, and scds separately to identify doublets in the dataset, with all algorithms executed using default parameters. Assuming an increase of 0.008 in the doublet rate for every additional 1000 cells. Based on the expected doublet rate, we assessed the classification of each cell by the three algorithms. A cell was considered a doublet and subsequently removed if it was classified as such by at least two of the algorithms. After quality control, 29,535 single cells from 2 samples and 17,453 features remained for downstream analysis.

Unsupervised clustering analysis and identification of cell types

We utilized the R package Seurat for comprehensive single-cell analysis. The expression matrix of the integrated dataset was normalized by the NormalizeData function with default parameters. The FindVariableFeatures function was applied with default parameters to detect 2,000 highly variable genes (HVGs) for the normalized matrix. The ScaleData function was used to scale the expression matrix with default parameters. The Top 30 PCs were calculated using the RunPCA function based on HVGs and the dimensionality of the dataset was reduced using the RunUMAP function. Nearest neighborhood graphs were built using the FindNeighbors function, and the community algorithm was applied for clustering using the FindClusters function with a resolution setting of 0.3. We first annotated the 10 major cell types identified in our dataset based on well-known marker genes We used the FindAllMarkers function to identify differentially expressed genes (DEGs) of each cell type as maker genes with adjusted $P < 0.05$ using Bonferroni correction.

We performed a second round of clustering to further characterize subpopulations of T cells and macrophages. Owing to the variable amount and property of cells in each major cell type, different parameters for clustering were used. For the clustering of T/NK cells, the top 25 PCs were selected based on 1,500 HVGs (resolution = 0.6). For macrophages, the top 30 PCs were selected based on 2,000 HVGs (resolution = 0.5).

Differential expression and functional annotation

We used the FindMarkers function based on the Wilcoxon rank-sum test to identify DEGs across two groups. P value adjustment was performed using Bonferroni correction. Genes with adjusted P values < 0.05 were considered as DEGs. Gene ontology analysis of DEGs was performed using the clusterProfiler R package. In the process of cell annotation, we summarized the list of characteristic genes that define T cell functions (including naive, cytotoxic, exhaustion, inflammatory, and resident signature) and macrophage functions (including M1 and M2 polarization, phagocytosis, and angiogenesis signature) in published studies. The scoring of cell function based on a specific gene set was performed through the AddModuleScore function.

Cell developmental trajectory

The lineage trajectory of T cells was applied by the Monocle2 algorithm with the marker genes of clusters. The cell differentiation trajectory was inferred with the default parameters of Monocle2 after dimension reduction and cell ordering. We also performed CytoTRACE analysis with a default parameter, an algorithm that predicts differentiation states from scRNA-seq data based on the simple yet robust observation that transcriptional diversity decreases during differentiation, to complement the trajectory analysis from Monocle2.

Flow cytometry analysis

The single cells resuspended in PBS were incubated with 2%BSA for 30 min to avoid nonspecific binding. Subsequently, the cells were stained with antibodies specific for cell surface markers and with Fixable Viability Dye eFluor™ 455UV (65-0868-18), and then incubated in permeabilization reagents (Invitrogen, 2430408) for 30min before staining with antibodies specific for intracellular markers according to the manufacturer's instructions. For mouse tumor samples, the single-cell suspensions were stained with the following antibodies: anti-CD45-Alexa Fluor™ 488 (Invitrogen, #53-0451-82), anti-CD3e-APC-eFluor™ 780 (Invitrogen, #47-0031-82), anti-CD8a-APC (Invitrogen, #17-0081-82), anti-PD-L1-Super Bright™ 436 (Invitrogen, #62-5982-82), anti-EpCAM-Super Bright™ 600 (Invitrogen, #63-5791-82), anti-Granzyme B-PE-Cyanine7 (Invitrogen, #25-8898-82), anti-Ki-67-PerCP-eFluor™ 710 (Invitrogen, #46-5698-82), anti-IFN-γ-PE (Invitrogen, #12-7311-82), anti-I-A/I-E (MHC-II)-PerCP-eFluor™ 710 (Invitrogen, #46-5321-82), anti-CD11b-APC (Invitrogen, #17-0112-81), anti-SPP1-PE (Invitrogen, IC808-P). For human blood samples, the single-cell suspensions were stained with the following antibodies: anti-CD45-Brilliant Ultra Violet™ 496 (Invitrogen, #364-0459-42), anti-CD3-Alexa Fluor™ 488 (Invitrogen, #53-0037-42), anti-CD8a-Super Bright™ 780 (Invitrogen, #78-0088-42), anti-CD4-Brilliant Ultra Violet™ 661 (Invitrogen, #376-0049-42), anti-Granzyme B-PE-Cyanine7 (Biolegend, #372214) and anti-IFN-γ-APC-eFluor™ 780 (Invitrogen, #47-7319-42). Flow cytometry was performed using BD LSRFortessa flow cytometer, and analysis was done using FlowJo V10.

RNA isolation and Real-time PCR

Total RNA was isolated from CT26 cells and mouse frozen tissues with Trizol reagent (TIANGEN, DP424). In brief, samples were homogenized in Trizol reagent and mixed. 200 μL of chloroform was added, gently mixed and incubated for 5 min on ice. After incubation, microcentrifuge tubes were centrifuged for 15 min at 12,000 g at 4 °C. The aqueous phase was transferred to new tubes. An equal volume of isopropanol was added and mixed with incubation on ice for 10 min. Samples were centrifuged at 12,000 g for 10 min at 4 °C. Aspirated off liquid and added 1mL of cold 75% ethanol to wash the pellet. The RNA pellet was air-dried for a few minutes at room temperature and subsequently resuspended in 20 μL of RNase-free water. The quantity and quality of RNA samples were determined by measurement using a NanoDrop Microvolume Spectrophotometers (Thermo Scientific, USA). The RNA samples with OD values of 260/280 $\geq$ 1.9 were selected for downstream analyses.

Reverse transcription reaction was performed in a SimpliAmp thermocycler (ThermoFisher, USA) using 5× PrimeScript™ RT Master Mix (Takara, RR036A) according to the manufacturer's protocol, under the following conditions: reverse transcription at 37°C for 15 min, heat inactivation at 85°C for 5 seconds and maintained at 4°C. Real-time PCR (RT-PCR) was carried out in a CFX Opus 96 Real-Time PCR System (Bio-Rad Laboratories) using iTaq™ Universal SYBR® Green Supermix (Bio-Rad, #1725120). The program contained three stages: 95 °C for 3 min, 40 cycles of 95°C for 10 s, 59°C for 30 s, and 72°C for 30 s.

Immunohistochemistry (IHC) and Immunofluorescence (IF) staining

Mouse tumor tissues were fixed in 10% buffered formalin, dehydrated and paraffin embedded. Antigen retrieval was achieved by boiling in 1 mM EDTA buffer (pH 9.0) for 15 min. Sections were blocked with goat serum and stained with primary antibody at 4 °C overnight. Sections were then stained with appropriate HRP or fluorescein-conjugated secondary antibodies at room temperature for 1 h. For IHC, sections were developed using 3,3′-diaminobenzidine (DAB) (CST, #11725S) and counterstained with hematoxylin. For IF, the slides were rinsed again with PBS and then incubated with nuclear dye.

Co-immunoprecipitations

Cells were lysed in Pierce IP Lysis Buffer (Beyotime, #P0013) and protease inhibitor cocktail. Then proteins were quantified using BCA Assay Kit (Solarbio, Beijing, China). For immunoprecipitation analysis, 500 μg of protein from cells were prepared. To preclear the sample, the samples were incubated with 20 μL of Protein A&G magnetic beads (Santa Cruz Biotechnology, #E1023) for 4h at 4 °C with constant rotation. Then 1 μg antibody was incubated with 30 μL agrose beads at 4 °C overnight with constant rotation. The agrose beads were then washed 3 times with IP buffer, and immunoprecipitated proteins were eluted from agrose beads by

1× loading buffer (Beyotime, #P0015A) and then were incubated at 99 °C for 10 min, centrifuge, taking the upper layer of liquid including immunoprecipitated protein to Western blot analysis.

PD-L1 lactylation-modified shotgun identification

Using the Filter-Aided Sample Preparation (FASP) method, the PD-L1 co-immunoprecipitation (Co-IP) sample was digested with trypsin buffer and incubated at 37°C for 16-18 hours. The Thermo Scientific EASY column (2 cm × 100 μm, 5 μm-C18) was equilibrated with 95% Solution A (0.1% formic acid in water). The sample was then loaded by an autosampler onto the Thermo Scientific EASY column (75 μm × 100 mm, 3 μm-C18) and separated at a flow rate of 300 nL/min. The liquid phase gradient was as follows:

0 to 50 minutes: Solution B (0.1% formic acid in acetonitrile, 84% acetonitrile) increased linearly from 4% to 50%.

50 to 54 minutes: Solution B increased linearly from 50% to 100%.

54 to 60 minutes: Solution B was maintained at 100%.

After desalting and separating the enzymatic digests using capillary high-performance liquid chromatography, mass spectrometry analysis was performed using the HF-X mass spectrometer (Thermo Fisher).

Targeted organic acid metabolomics

Weigh an appropriate amount of organic acid standard and prepare a single standard mother solution with methanol or water. Measure an appropriate amount of each mother liquor to prepare a mixed standard, and dilute it with 30% methanol-water (0.1% FA) to an appropriate concentration to prepare a working standard solution. The mother liquor and working standard solution were kept refrigerated. Appropriate samples were taken into a 2 mL centrifuge tube, and 500 μL of 30% methanol aqueous solution (containing 0.1% formic acid) was accurately added and swirled for 60 s. Add 2 steel balls. Put into the tissue grinder, grind at 55 Hz for 1 min, repeat the above operation at least twice; Centrifuge at 12000 rpm for 10 min at 4°C. Appropriate amount of the supernatant was added to 30% methanol aqueous solution (containing 0.1% formic acid) and diluted 5 times. The supernatant was swirled for 30 s. The supernatant was passed through 0.22μm filter membrane, and the filtrate was added to the test bottle for analysis.

Procedures for clinical trial

The clinical trial (ChiCTR2300067929) is a single-arm, phase I study. Due to the lack of −SG food suitable for cancer patients on the market, Recovery Plus Clinic Co. has developed and produced the −SG nutritional powder. This product has been approved for use in tumor patients requiring nutritional therapy, with the Food Production License Number SC12751010750003 and Product Standard Number GB/T 29602. Each 100g of nutritional powder contains 1978KJ of energy (RNV 24%), 16.6g of protein (RNV 28%), 22.2g of fat (RNV 37%), 49.4g of carbohydrates (RNV 16%), 4.32g of dietary fiber (RNV 17%), and various vitamins and minerals. This study used 30 kcal/kg/day of energy and 1.5 g/kg/day of protein as standards to calculate the required fluid intake for patients. We use the nutrient powder and low amino acid fruits and vegetables within our regulations to replace the normal diet, without interfering with the standard anti-tumor treatment that patients need to undergo according to the existing guidelines. Researchers conducted daily follow-up to record patients' intake and closely monitor their adverse reactions. Once serious adverse reactions occur or BMI<18.5 or BRS-2002 score $\geq$ 3, we will restore the patient's normal diet and provide additional nutritional supplements.

Peripheral blood samples were collected at baseline and then every 3 weeks for at least 9 weeks (3 cycles) after the treatments began. Serum was collected for amino acid content determination and peripheral blood mononuclear cells (PBMCs) were isolated using Human Lymphocyte Separation Medium (Dakewe biotech, #7211011). Additionally, routine CT, MRI scans, and endoscopic examinations were performed according to clinical evaluation requirements. The primary outcomes were safety and levels of serum amino acids. Secondary outcomes were tolerability, tumor volume and the effects on immune cells.

QUANTIFICATION AND STATISTICAL ANALYSIS

The sample size for this study was calculated using PASS software version 15.0.5. The primary safety endpoint is the incidence of adverse events, with expected rates at 60%. The type I error rate (α) is set at 0.05, and the power (1-β) is 0.85. The effective sample size needed is 32 participants. Considering an anticipated dropout rate of 20%, the total sample size required is 40 subjects.

The two-side unpaired Student's t-test was used for two-group comparisons of values. Comparisons of tumor growth curves were performed by a two-way ANOVA test followed by Tukey's multiple comparison test. A linear regression model (Pearson's correlation) was used to determine the individual correlations between different variables. All analyses were finished using the GraphPad Prism 8 software (GraphPad Software Inc., San Diego, CA, USA). All the error bars represent the standard error of the mean (SEM). P-values < 0.05 were considered significant: *$P < 0.05$; **$P < 0.01$; ***$P < 0.001$; ****$P < 0.0001$. Unless otherwise indicated, the asterisks indicate the statistical comparison to the control group.